

Award Accounts

The Chemical Society of Japan Award for Technical Development for 2003

Development of Self-Assembling Nucleators for Highly Transparent Semi-Crystalline Polypropylene

Toshiaki Kobayashi* **and Takeji Hashimoto**[1]

Research and Development Division, New Japan Chemical Co.,
13 Yoshijima, Yagura-Cho, Fushimi-Ku, Kyoto 612-8224

[1]Department of Polymer Chemistry, Graduate School of Engineering, Kyoto University,
Katsura, Nishikyo-ku, Kyoto 615-8510

Received August 6, 2004; E-mail: sol_kobayashi@yahoo.co.jp

In 1,3:2,4-bis-*O*-(*p*-methylbenzylidene)-D-sorbitol (PDTS)/molten i-PP systems, the self-assembling ramified fibrils of PDTS are formed at $T_{fg,c}$ higher than T_c during the cooling process. They function as the nucleators for the nucleation of molten i-PP. The ramified fibrils have the following characteristics: i) hexagonal crystal with the lattice cell $a = b = 30.2$, $c = 4.4$ Å, and $\gamma = 120^\circ$, ii) mass fractal structure with large specific surface area, and iii) random orientation. Thus the following properties are induced for the i-PP: i) excellent transparency so that the lamellae build a sheaf-like crystalline superstructure with a small apex angle, ii) iso-directional and improved mechanical properties, and iii) shortened molding time.

Stereo-specific polypropylene (i-PP) is known among commodity polymers as one with low density and balanced mechanical and thermal properties. As i-PP also harmonizes with the environment, 30 million tons were used in the world and 2.5 million tons were used in Japan in 2001. From industrial view points, some kinds of nucleating agents (nucleators) have been used as additives in order to increase the nucleation rate of molten i-PP in mold-processing. The nucleator plays a role of decreasing[1] the free energy, ΔG, for nucleation of molten polypropylene, resulting in the increase of nucleation temperature of molten i-PP, T_c, in the mold-processing, that is, decrease of super-cooling for nucleation $\Delta T = T_m - T_c$, where T_m is melting temperature of i-PP. The number of spherulites of i-PP increases, and hence their size decreases.[1] The mechanical strength and thermal distortion temperature of the i-PP sheet also enhance.[1] Some representatives of industrial nucleators are talc, clay, hydroxyaluminium bis(*tert*-butylbenzoate), sodium *tert*-butylbenzoate, and sodium 6,6-methylenebis(2,4-*tert*-butylphenyl)phosphate, where the particles have large aspect ratio or square-planar form. These nucleators belong to the classical type, where their particles act as "seeds for nucleation" in the process of heterogeneous nucleation of molten polypropylene.

Classical nucleators have the following three limitations or weak points: i) the particles should have the limit of minimum size depending on the mechanical methods of crushing and sieving, the problem of auto-aggregation between small particles in their storage, and the risk of powder-explosion. ii) As the particles of nucleators tend to align along the flow direction (MD) of molten i-PP, the i-PP sheet with skin and core double layers is obtained[2] by the mold-processing. The degree of crystalllite-orientation of i-PP is different in the two layers, and the i-PP sheet shows different crystallite-orientation in MD, TD, and ND directions. Therefore the i-PP sheet or film sometimes causes serious problems such as anisotropic mechanical properties and anisotropic shrinkage, resulting in the collapse of their shape during their storage. And iii) transparency of the i-PP sheet is not clearly increased because of the scattering due to the disparity of refractive index between nucleators and i-PP and the anisotropy of crystallite-orientation, in addition to the inherent scattering based on the differences of the refractive indices between crystal and amorphous regions of the i-PP sheet.[3]

Some kinds of low-molar-mass-molecules (defined hereafter as small-molecules) self-assemble into a percolation network from homogeneous solution composed of small-molecules and organic solvent, resulting in gel formation of the systems. The percolation network usually has a large specific surface area. Therefore the three problems of classical nucleators were expected to be solved by using self-assembling type nucleators in place of classical ones. A series of sorbitol-acetal chemicals, which are small-molecule gelators, are expected to have excellent properties as nucleators for i-PP based upon the following reasons: i) 1,3:2,4-bis-*O*-(*p*-methylbenzylidene)-D-sorbitol (PDTS) molecule forms self-assembly ramified fibrils[4] with diameter of 10 nm at higher temperature than T_c during cooling process of homogeneous PDTS/molten i-PP system, and hence the ramified fibrils with large specific surface area can be ide-

Published on the web February 11, 2005; DOI 10.1246/bcsj.78.218

ally obtained in situ. ii) As the structure of ramified fibrils is isotropic, having random orientation, the i-PP sheet containing PDTS nucleator will show random crystallite-orientation of i-PP. Thus the i-PP sheet or film was expected to have isotropic mechanical properties and shrinkage. iii) The transparency of the i-PP sheet should be excellent so that the scattering from the ramified fibrils and the scattering based on the anisotropic crystallite-orientation of the i-PP sheet are minimized. And iv) since PDTS molecules form in situ self-assembled ramified fibrils, the process control of molding of i-PP was expected to be simplified. Thus we focused on a series of sorbitol-acetal chemicals, which form transparent gels[4] in molten polymers and various kinds of solvents, accompanied by sol–gel phase transition.

A series of sorbitol derivatives, which we named self-assembling type nucleators, have been developed based on their self-assembling properties[3] in molten polymers. Among the self-assembling type nucleators, we found that 1,3:2,4-bis-*O*-(*p*-methylbenzylidene)-D-sorbitol (PDTS) increases not only the rate of nucleation of molten polypropylene but also improves dramatically the transparency[5] of i-PP sheets.

At a first development stage, we studied sol–gel transition of PDTS in liquid matrix in order to elucidate the self-assembling processes and their structures. Let us survey physical sol–gel phase transitions for small-molecule gelators and solvent or molten polymer systems.

Flory,[6] de Gennes,[7] and Staufer[8] et al. defined gels as materials having a three dimensional infinite network structure which includes solvents or molten polymers in it. Gels have characteristic rheological properties as soft elastic materials. Gels can be classified in the following two groups: chemical gels and physical gels. The chemical gels are made of chemically cross-linking bonds. Chemical polymer gels have the cross-linking bonds formed by chemical reactions between polyfunctional monomers, polyfunctional oligomers, and polymer chains. Physical gels include polymer gels and low-molar-mass-molecule gels (defined hereafter as small-molecule gels). The physical polymer gels, which are made of physically cross-linking bonds, are composed of two types, depending on whether or not phase separation occurs in the gelation process. The gels with phase-separated structures in them are formed by liquid/liquid (L/L) phase separation into a co-continuous structure composed of domains rich in polymers and poor in polymers, followed by vitrification[9] or solid/liquid (S/L) phase transition in polymer-rich domains. The other type of gels has physical network structures formed only by S/L phase transitions. Small-molecule gels are made of continuous network structures of gelling molecules in 3D space formed by their physical associations. Physical gels are usually thermoreversible.

The physically cross-linking bonds in small-molecule gels will be formed by intermolecular associations into fibrils by hydrogen bondings, Coulombic forces, and hydrophobic bonds.[10]

T_{fg} and Φ_{fg} are respectively defined as critical temperature and critical concentration of gelators where the systems undergo sol to gel or gel to sol phase transition. ΔT and $\Delta\Phi$ respectively means a quench depth from T_{fg} at a given concentration Φ and that from Φ_{fg} at a given temperature T. We consider the time evolution of the physical gelation in the parameter space of T and Φ. The distance of our observation point from the gel point, ε, is defined by

$$\varepsilon \equiv |p - p_c|/p_c, \tag{1}$$

where p is the conversion of the monomer to cluster before or after the gel point and p_c is p at the gel point, respectively.

Gelation is described as a critical phenomenon at $\varepsilon = 0$ ($p = p_c$) or $\varepsilon \to 0$ ($p \to p_c$) and hence by the following scaling laws with respect to ε:[11]

$$\xi \sim \varepsilon^{-\nu}, \tag{2}$$

$$M_w \sim \varepsilon^{-\gamma}, \tag{3}$$

$$M_{max} \sim \varepsilon^{-1/\sigma}, \tag{4}$$

$$\eta_0 \sim \varepsilon^{-k}, \tag{5}$$

in the case of $p < p_c$, and

$$G_\infty \sim \varepsilon^{z}, \tag{6}$$

$$P \sim \varepsilon^{\beta}, \tag{7}$$

in the case of $p > p_c$. Here ξ, M_w, M_{max}, η_0, G_∞, and P are the maximum radius of clusters, the average molecular weight of clusters, the mass of the maximum cluster, the zero-shear viscosity, the equilibrium modulus, and the probability that monomer interconnects with an infinite cluster (gel fraction), respectively. ν, γ, $1/\sigma$, k, z, and β are critical exponents of the respective quantities. M_{max} and ξ are interrelated by

$$M_{max} \sim \xi^{d_f}, \tag{8}$$

where d_f is a mass fractal dimension. It should be noted that ξ, M_w, M_{max}, and η_0 diverge when $\varepsilon \to 0$ from the sol state, though G_∞ and P converge upon zero[11] when $\varepsilon \to 0$ from the gel state.

There have not been many reports on the physical small-molecule gels compared with physical polymer gels, and only a limited number of small-molecules, such as 12-hydroxyoctadecanoicacid,[12] dibenzylidene sorbitol,[13] steroid derivatives,[14] and metal salts of fattyacid,[15] have been known as small-molecule gelators.

Many researchers have attempted to synthesize more useful and superior small-molecule gelators for organic solvents or water, resulting in the invention of various kinds of small-molecule gelators in recent years. Representatives include 3,4-dimethylbenzylidenesorbitol,[16] steroid derivatives, D-galactose derivatives,[17] arylcyclohexanol derivatives,[18] *N*-acylamino acids,[19] longalkylaldonamides,[20] lecithin,[21] calixarenes,[22] longalkylamines and their quarternary ammonium halide salts,[23] acyclic alkanes with one hetero atom such as bisalkyl thioethers or dioctadecylamine,[24] and aminoaryl ethers of sugar-based acetals.[25] A small amount of gelators, from 0.2 to 6 wt %, associate themselves to form 3D networks in the solvents, resulting in formation of gels with finite yield stress. As a consequence the systems lose macroscopic fluidity. Moreover, every small-molecule gelator has amphiphilic characteristics, having both hydrophilic and hydrophobic parts within a molecule.

There have been many studies to construct phase diagrams for various kinds of small-molecule gelator and solvent sys-

tems in the parameter space of T and Φ in order to determine T_{fg} and Φ_{fg}. Many research projects have been devoted to study enthalpy change,[26] ΔH, and entropy change, ΔS, accompanied by the sol–gel phase transition. The network structures in gels have also been investigated. In these studies,[27,28] it was found that intermolecular hydrogen bonding interactions take place between the small-molecule gelators, resulting in the formation of the network structures of fibers or sheets made of gelators. Several small-molecule gelators, such as 12-hydroxy octadecanoic acid[12] or a cyclic bis-urea,[27] show interesting characteristics of polymorphism: the crystal form of a gelator itself and the crystal form of the fibrous network structures self-assembled by the sol–gel transition are different.

We investigated the following three items: dynamics of self-assembling process of PDTS molecules in gel formation process, gel morphologies which are filled with amorphous liquid, and phase diagrams of the systems in the parameter space of T and Φ_{PDTS}. Subsequently, we developed the self-assembling nucleator of PDTS for highly transparent i-PP based upon a new usage of the self-assembling gelators. Results shall be investigated based on theories such as percolation theory for sol–gel phase transition, spinodal decomposition (SD) theory for phase separation, scattering method, nuclear magnetic resonance (NMR) spectroscopy, and computer calculations for configuration and conformation of a PDTS molecule with MOPAC2000[29] based on molecular orbital theory.

In this paper, we selected PDTS among a series of sorbitol-acetals with function of self-assembling nucleators as the one which induces the highest transparency of the i-PP sheet. We will describe the self-assembling process of PDTS in Sec. 1. In Sec. 1.1, the stereo structure of a PDTS molecule is presented. In Sec. 1.2, the PDTS/*n*-dibutylphthalate (DBP) system was used as a typical model system having the interplay of the two kinds of phase transitions. We investigate the self-assembled structure in the PDTS/DBP system as a function of T and Φ_{PDTS} and the dynamics of the self-assembling processes via liquid–liquid phase separation and sol–gel transition. In Sec. 1.3, we investigate time-evolution of shear moduli in the physical gelation process of PDTS in polystyrene melt. At the gel point, we elucidate that storage and loss shear moduli, G' and G'', are described by the power law of frequency ω, $G' \sim G'' \sim \omega^n$, with the critical exponent n equal to $2/3$, in agreement with the value predicted by the percolation theory. The exponent n and the gel strength S at the gel point were measured as a function of quench depth ΔT. We will directly prove the self-similarity of evolving structures from in-situ and real time structure analysis during the gelation process. We will also compare fractal dimensions obtained from structure factors and the viscoelasticity of gel networks of PDTS at gel point. In Sec. 2, hierarchical structures of PDTS gel will be discussed. In Sec. 3, we will describe the self-assembling nucleator of PDTS for highly transparent i-PP. In Sec. 3.1, we investigate dynamic viscoelasticity of the PDTS and molten i-PP systems in a wide temperature range across the sol–gel transition temperature. In Sec. 3.2, we characterize wide-angle X-ray diffraction (WAXD) profiles of the i-PP sheet. In Sec. 3.3, we clarify the morphology of i-PP induced by the self-assembled structure of PDTS. In Sec. 3.4, the concentration dependencies of the self-assembled structure of PDTS upon properties of the i-PP sheet are exhibited. In the final Sec. 4, we will draw some conclusions of these studies.

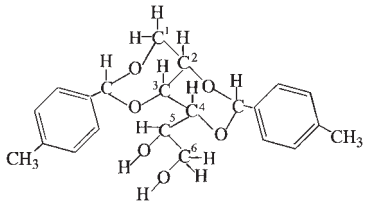

Fig. 1. Stereostructure of 1,3:2,4-bis-*O*-(*p*-methylbenzylidene)-D-sorbitol molecule.

1. Self-Assembling Process of PDTS

1.1 The Stereostructure of a PDTS Molecule. 1,3:2,4-Bis-*O*-(*p*-methylbenzylidene)-D-sorbitol (PDTS) was synthesized from D-sorbitol and *p*-methylbenzaldehyde, and the positions of two acetal-rings carrying each benzylidene substituent and the conformation of two 1,3-dioxane rings were made clear.[30] Figure 1 shows the stereostructure of a PDTS molecule. The analysis of ^{1}H NMR data included correlated spectroscopy (COSY) data and nuclear Oberhauser enhancement and exchange spectroscopy (NOESY) data for a PDTS molecule. Such analyses showed that two *p*-methylphenyl substituents occupy the equatorial position and two 1,3-dioxane rings are connected in a *cis*-*O*-inside way. Figure 2 shows the spectrum of NOESY for a PDTS molecule. The number of nuclear Overhauser effects (NOE) between methine-proton of benzylidene substituents at chemical shift $\delta = 5.60$ and protons of dioxane rings is four couples, indicating the all coupled protons occupy *cis*-positions to each other. The molecular mechanics of force field calculation supported[30] this stereostructure and further revealed that the two aryl rings for 2,4-*O*-acetal and 1,3-*O*-acetal have the torsion angle Φ_1 and Φ_2 of 130 and 71 degrees, respectively, in the most stable conformation of PDTS. The distances of the apse line between the end of two *p*-methyl substituents and the minor axis between the end of methylene of carbon 1 and the hydroxy substituent bonded to carbon 6 are 13.4 and 8.1 Å, respectively. The positions of acetals as well as the *cis*-junction of two dioxane rings are reasonable, based upon the configuration of D-sorbitol. The mechanism of acetalization reaction of D-sorbitol and *p*-methylbenzaldehyde is described in detail elsewhere.[31]

1.2 Self-Assembly of the PDTS/*n*-Dibutylphthalate (DBP) System.[32] We investigated the self-assembled structure of PDTS/DBP system in the parameter space of T and Φ_{PDTS}. Optical microscopic studies revealed that the phase diagrams can be divided into four regions, as shown in Fig. 3. Region I is in the homogeneous solution and region II is in the sol state, where the solution still has fluidity and contains micro-gels composed of a coarse spherulitic texture. Regions III and IV are in gel state. In region III, PDTS molecules form the volume-filling spherulites in the system. In region IV, both the L/L phase separation process and the S/L transition of the PDTS molecules are involved in the self-assembling processes. Figure 4 shows typical OM images in each region. The network structures of the gel in regions III and IV were investigated using combined light scattering (LS), ultra-small-angle X-ray scattering (USAXS), and small-angle X-ray scattering

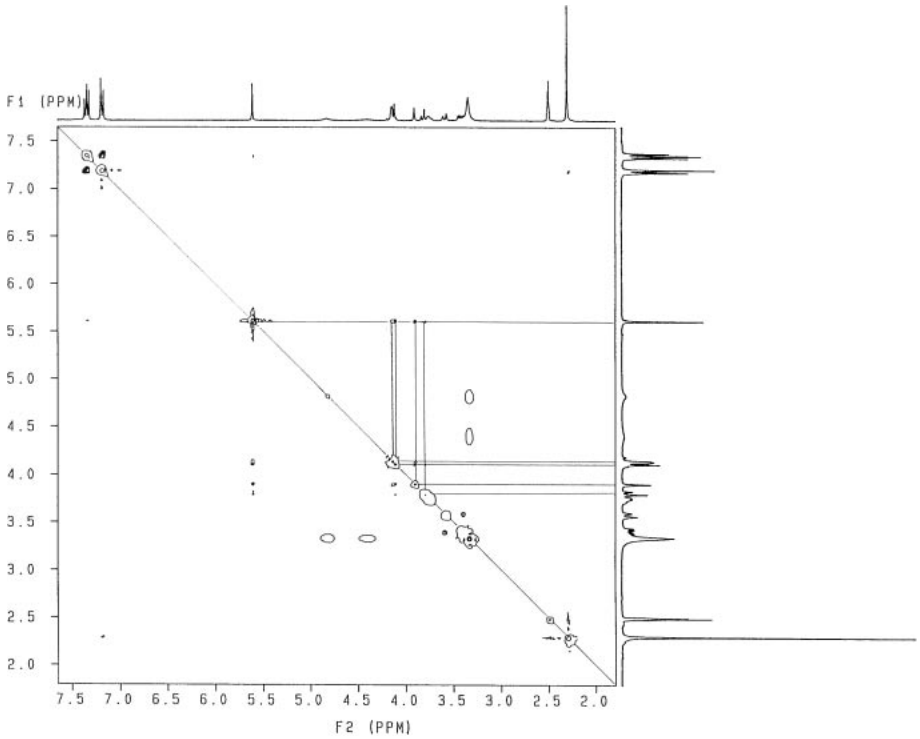

Fig. 2. Two dimensional ^{1}H–^{1}H NMR spectrum of NOESY for PDTS molecules. Four couples of nuclear Overhauser effect can be found between two benzylidene acetal methines (chemical schift $\delta = 5.60$) and carbon 1-H ($\delta = 4.12$ or 4.17), carbon 2-H ($\delta = 3.91$), carbon 3-H ($\delta = 4.11$), and carbon 4-H ($\delta = 3.82$).

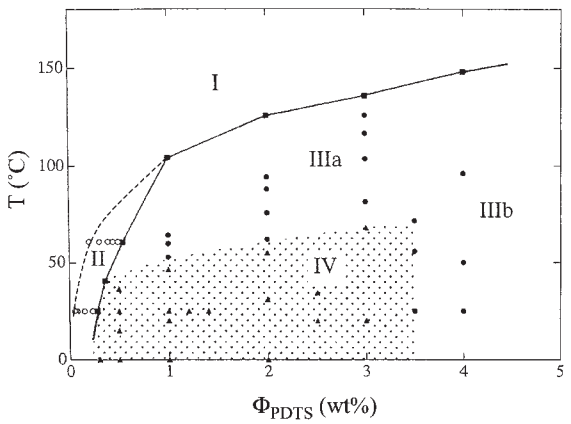

Fig. 3. Phase diagram of PDTS/DBP system in the parameter space of temperature, T and composition, Φ_{PDTS}. The sol–gel transition points obtained from cooling processes are indicated by filled squares. Open circles indicate the points where sols with microgels are observed. The thick solid lines connecting the filled squares are for the visual guide. Filled circles indicate the points where only spherulites are observed, while filled triangles indicate the points where periodic bicontinuous patterns are observed. The parameter space was divided into regions I to IV as indicated in the figure.

(SAXS) methods. Figure 5 shows the results for region III (4.0 wt % PDTS/DBP measured at 25 °C) and IV (0.5 and 1.0 wt % PDTS/DBP measured at 25 °C). Ramified structures made of PDTS fibrils in regions III and IV were characterized by the values of the mass fractal dimension d_f and by both the upper cut-off length scale and the lower cut-off length scale of the fractal ramified structures. In the case of 1.0 wt % PDTS/DBP gel, since the scattering intensity is expressed by a power law q^{-n} with the exponent $n = 2.5$ between the lower cut-off wavenumber 5.3×10^{-4} nm^{-1} (point B) and the upper cut-off wavenumber 0.4 nm^{-1} (point C), the PDTS crystalline fibrils form a self-similar mass fractal structure with $d_f = 2.5$, having both the upper cut-off length scale of $\Lambda = 11.9$ μm and the lower cut-off length scale of $\Lambda = 15.7$ nm.[32] Next, we explored whether the change in $I(q,t)$ with t of the time-resolved light scattering for the phase-separation of the system, quenched in region IV, could be approximated with the Cahn's linearized theory[33] in the early stage SD expressed by Eqs. 9 and 10.

$$I(q,t) = I(q,0)\exp[2R(q)t]. \tag{9}$$

Here $R(q)$ is given by

$$R(q) = D_{app}q^2\left[1 - \frac{q^2}{2q_m^2(0)}\right], \tag{10}$$

where D_{app} and $q_m(0)$ are, respectively, the interdiffusion coefficient and the characteristic wave number for the concentration fluctuations developed in the early stage SD. Figure 6 shows a change in the scattering intensity profile $I(q,t)$ with time for 0.38 wt % PDTS/DBP quenched from 150 °C to 23 °C in region IV. Figure 7 shows clearly the change in $I(q,t)$ with time at fixed q's; these data were obtained from Figure 6. The linear relationship between $\ln[I(q,t)]$ vs t can be seen up to ~40 s, indicating that the time evolution of the structure factor in the short time limit satisfies Eq. 9. We estimated $R(q)$ from the slope of the plot to obtain the charac-

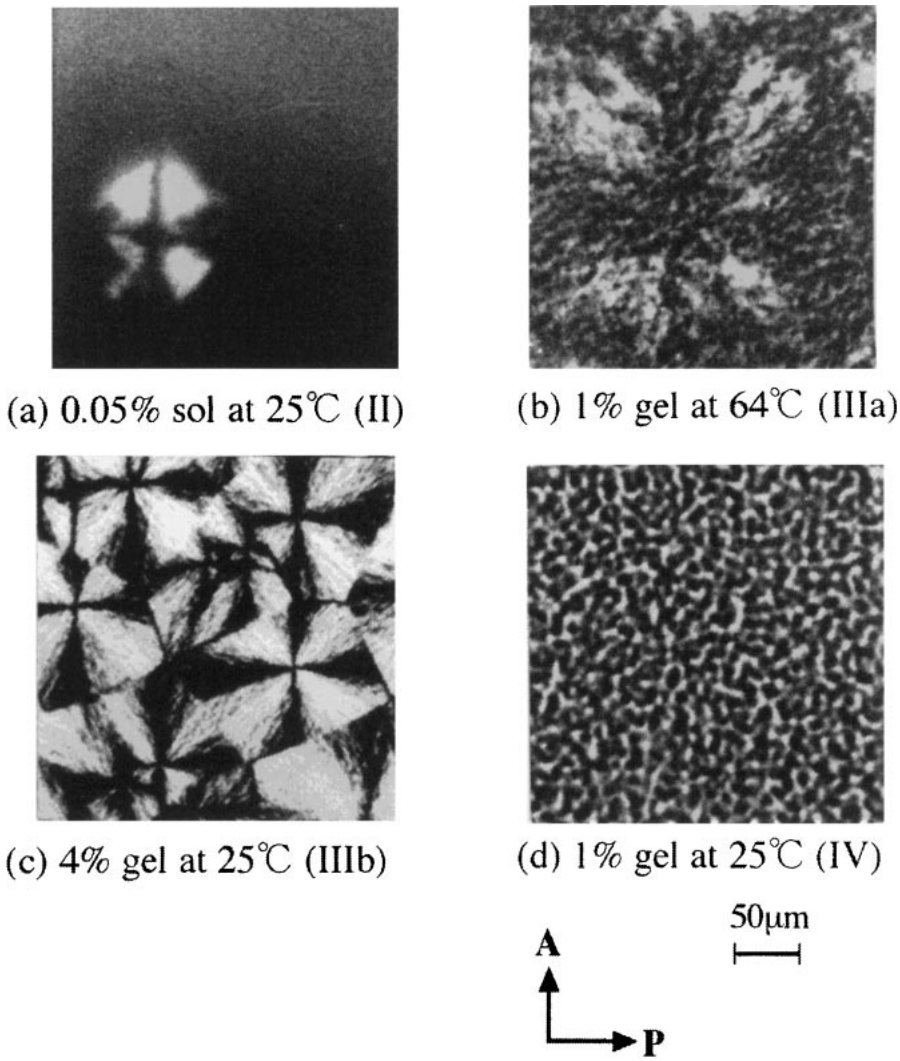

Fig. 4. Typical OM images in (a) region II (0.05 wt % PDTS/DBP sol at 25 °C), (b) region IIIa (1.0 wt % PDTS/DBP gel at 64 °C), (c) region IIIb (4.0 wt % PDTS/DBP gel at 25 °C), and region IV (1.0 wt % PDTS/DBP gel at 25 °C) under crossed nicols. The directions of analyzer and polarizer are indicated by the arrows A and P, respectively.

teristic parameters of D_{app} and $q_m(0)$. In Fig. 8, we plot $R(q)/q^2$ as a function of q^2 and evaluate D_{app} as $(9.93 \pm 0.22) \times 10^5$ nm^2/s and $q_m(0)$ as $(5.34 \pm 0.15) \times 10^{-4}$ nm^{-1} from the intercept and the slope, respectively. The plot shows the linearity as described by Eq. 10 within the experimental accuracy. The validity of Eq. 9 for the time changes in the scattered intensity and that of Eq. 10 for the linear relationship between $R(q)/q^2$ and q^2 indicate that the self-assembling process in the PDTS/DBP system at $t < 40$ s can be approximated by the linearized theory and that the origin of the periodic structure is the phase separation between PDTS and DBP via SD. We found that a bicontinuous phase-separated structure is first formed by L/L phase separation via SD in this region. The subsequent S/L transition of the PDTS in the PDTS-rich domain forms percolating crystalline fibrils, resulting in the gelation and the pinning of further growth of the bicontinuous structure via SD. Thus the gel preserves the memory of the periodical concentration fluctuation of PDTS developed during SD process, that is, the frozen periodical length, Λ_m, in itself. Subsequently the Φ_{PDTS} dependence of Λ_m was discussed. Figure 9 shows OM images, 2D Hv-LS patterns, and 2D Vv-LS patterns for the self-assembled structures for several concentration PDTS/DBP systems in region IV at 25 °C. According to the Cahn theory, the quench depth dependence of $q_m(0)$ is described by

$$q_m(0) = (3/R_0)[(T_s - T)/T_s]^{1/2}, \quad (11)$$

where R_0 is the averaged-radius of molecules in the system and T_s is the spinodal temperature for the liquid–liquid phase separation. Since Φ_{PDTS} in region IV is lower than 3.5 wt %, Φ_{PDTS} seems lower than that of critical point, at which the spinodal line and the binodal line in the parameter space of T and Φ_{PDTS} agree. As T_s decreases with decreasing of Φ_{PDTS}, the values of $q_m(0)$ are expected to decrease with decreasing Φ_{PDTS} at a given T and hence the Λ_m is expected to increase, being consistent with the experimental observation shown in Fig. 9. Consequently, the value of Λ_m is effectively controlled by the size of the concentration fluctuation of $q_m(0)$. Thus, the Φ_{PDTS} dependence of Λ_m at a fixed T can be predicted by the concentration dependence of $q_m(0)$ via the concentration de-

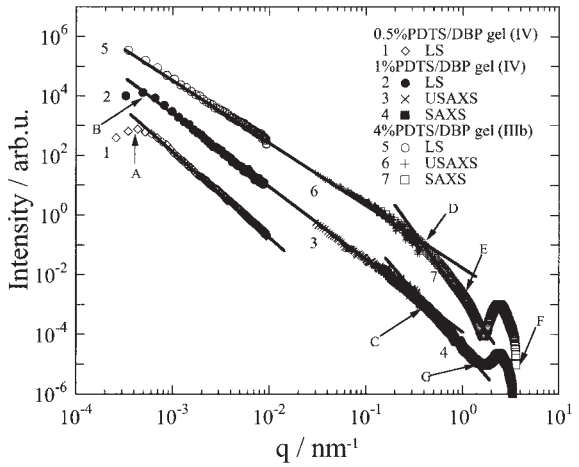

Fig. 5. Scattered intensity profiles of V_v-LS (profile 1) for 0.5 wt % PDTS/DBP (region IV), those of V_v-LS (profile 2), USAXS (profile 3) covering from $q = 0.03$ to 0.35 nm^{-1}, and SAXS (profile 4) covering from $q = 0.15$ to 2.8 nm^{-1} for 1.0 wt % PDTS/DBP (region IV), and those of V_v-LS (profile 5), USAXS (profile 6) covering from $q = 0.03$ to 0.35 nm^{-1}, and SAXS (profile 7) covering from $q = 0.15$ to 2.8 nm^{-1} for 4.0 wt % PDTS/DBP (region IIIb). For 1.0 wt % and 4.0 wt % PDTS/DBP systems, USAXS and SAXS profiles are shifted vertically so that they can be smoothly interconnected with the V_v-LS profiles. Note that the USAXS and SAXS profiles are overlapping over a sufficiently large q-range.

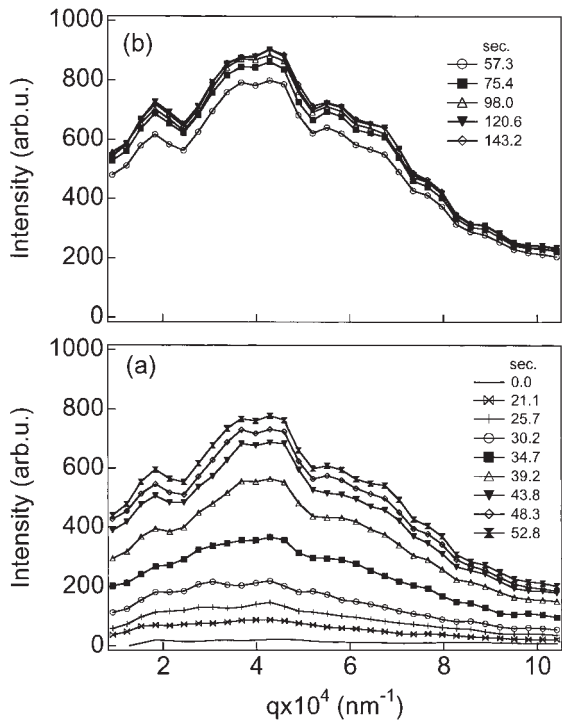

Fig. 6. Change in the V_v-LS profiles with time for 0.38 wt % PDTS/DBP (region IV) after the quench from 130 °C to 23 °C.

pendence of T_s, being controlled by the early stage of SD. The temperature dependence of Λ_m was also discussed. The characteristic time t_c is the parameter characterizing the coarsening

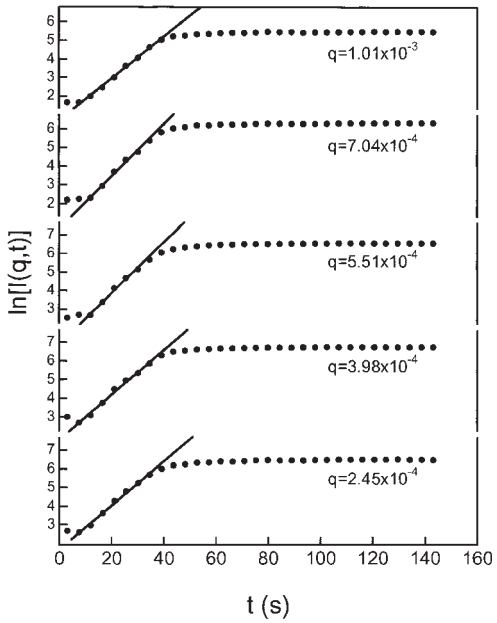

Fig. 7. Ln[$I(q, t)$] obtained from the data shown in Fig. 6 plotted as a function of t at fixed q's for 0.38 wt % PDTS/DBP at 23 °C.

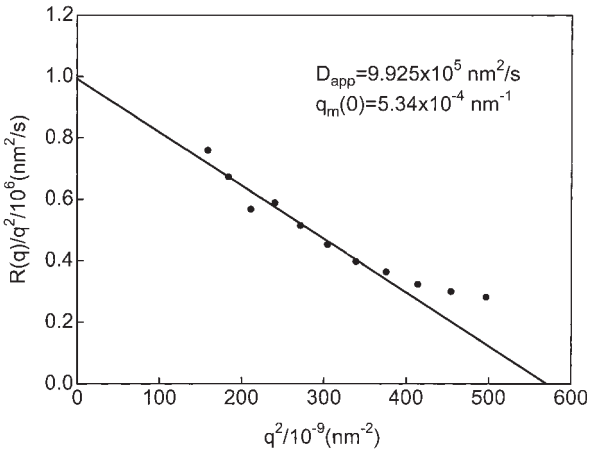

Fig. 8. $R(q)/q^2$ vs q^2 plot for 0.38 wt % PDTS/DBP at 23 °C.

rate of the phase-separated structures, and t_c defined by

$$t_c = 1/[q_m{}^2(0)D_{app}], \tag{12}$$

where D_{app} is given by

$$D_{app} = D(T)[(T_s - T)/T_s] \tag{13}$$

with $D(T)$ being the average self-diffusion coefficient of the molecules in the system. Substituting Eqs. 12 and 13 into Eq. 11, we found

$$t_c \sim D(T)^{-1}[(T_s - T)/T_s]^{-2}. \tag{14}$$

From Eq. 14 the coarsening occurs quickly with the increase of quench depth at a given Φ_{PDTS}. This fact is inconsistent with the experimental observations where Λ_m decreases with the increase of quench depth at a given Φ_{PDTS}. On the other hand, the growth rate of the crystallization is a function of supersaturation of PDTS and hence super-cooling of PDTS,

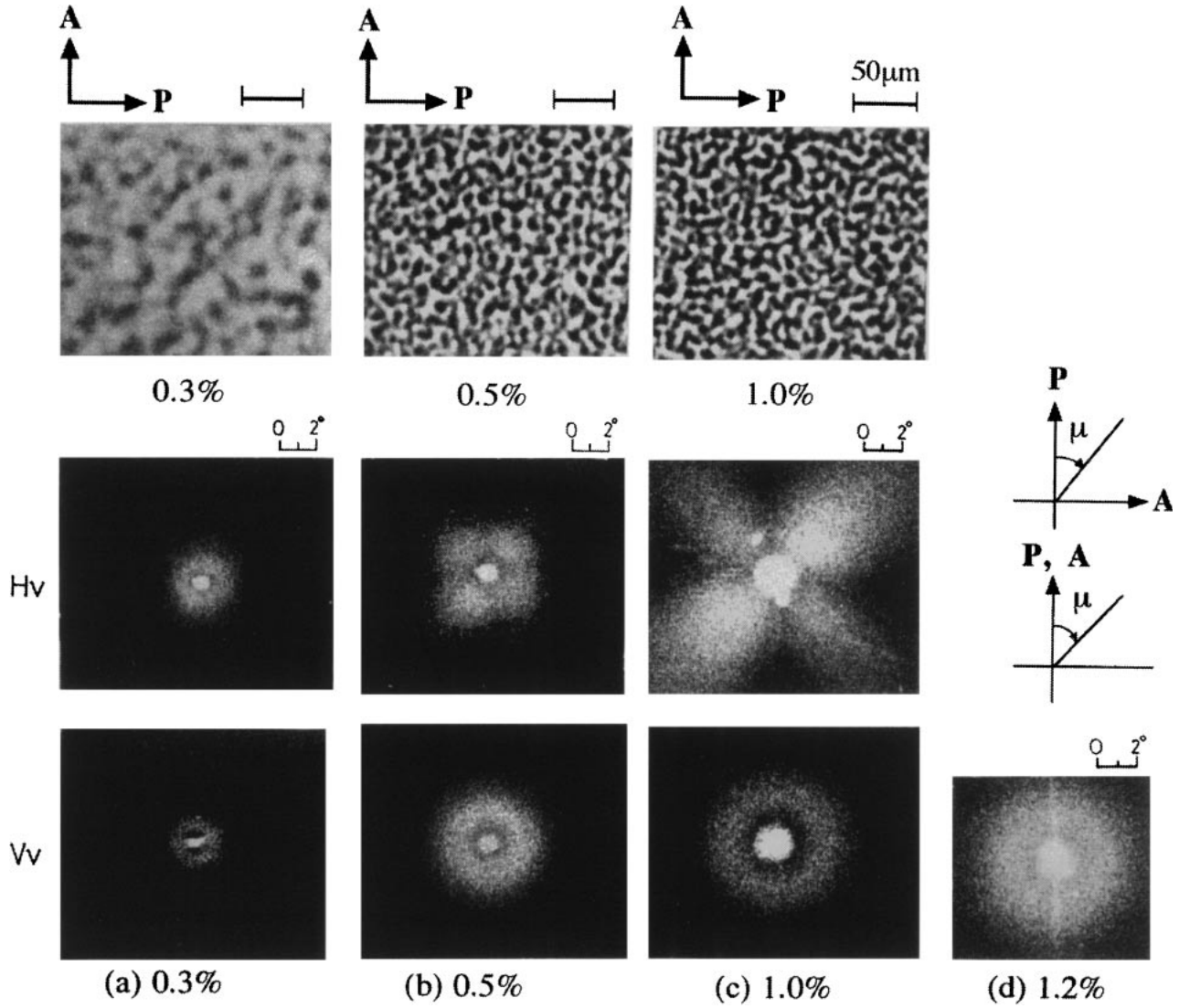

Fig. 9. OM images (upper row), 2D H_v-LS patterns (middle row), and 2D V_v-LS patterns (lower row) for the self-assembled structures for (a) 0.3, (b) 0.5, (c) 1.0, and (d) 1.2 wt % PDTS/DBP systems at 25 °C. The polarization directions of analyzer and polarizer for Hv and Vv scattering are indicated by the arrows A and P, respectively. The azimuthal angle μ is also defined in the figure.

$(T_{fg} - T)/T_{fg}$. The deeper the quench depth at a given Φ_{PDTS}, the faster the crystallization rate and hence the faster the freezing of phase-separated structures, resulting in smaller Λ_m at an earlier time of the early stage SD. Thus the temperature dependence of Λ_m at a fixed Φ_{PDTS} is controlled by the rate of crystallization of PDTS molecules.

1.3 Time-Evolution of Shear Moduli in the Physical Gelation Process of PDTS in Polystyrene Melt and Structure Factor at Gel Point.[34] We investigated the time-evolution of shear moduli at 183, 181, and 178 °C in a physical gelation process of PDTS in polystyrene melt. The weight-averaged molecular weight M_w and heterogeneity index M_w/M_n of PS are, respectively, 6.4×10^4 and 1.03, where M_n is the number-average molecular weight. The concentration of PDTS in PDTS/PS is 2.5 wt %.

Before gelation point, the steady state compliance J_e^0, and the terminal relaxation time can be scaled as

$$J_e^0 \sim \varepsilon^{-z}, \tag{15}$$

and

$$\tau \sim \eta_0 J_e^0 \sim \varepsilon^{-(k+z)}. \tag{16}$$

In polymer systems where hydrodynamic interactions are completely screened out (corresponding to Rouse limit) and the excluded volume effects are dominant, the critical exponents k and z are given by[35,36]

$$k = \nu(d_f + 2 - d), \tag{17}$$

$$z = \nu d, \tag{18}$$

with d_f and d (= 3 in our case) being the fractal dimension and space dimensionality, respectively. On the other hand, if excluded volume effects as well as hydrodynamic interactions are completely screened out, k is expressed by

$$k = \nu(\bar{d}_f + 2 - d) \tag{19}$$

with

$$\bar{d}_f = \frac{2d_f}{d+2-2d_f}, \tag{20}$$

while z has the same form as Eq. 18.

At gel point ($p = p_c$), the stress relaxation modulus $G(t)$, G', and G'' show the following power law behavior:[37]

$$G(t) = St^{-n}, \tag{21}$$

and

$$G' \sim G'' \sim \omega^n, \tag{22}$$

where gel strength S characterizes the strength of the gel at gel point. It should be noted that the power law behavior is limited to a finite frequency range due to the characteristic time of building block of the gel. Moreover, the power law behavior for physical gels should be more limited than that for chemical gels because of a finite life time of the physical bonds.[37] According to the theory of linear viscoelasticity,[38]

$$G'(\omega) = \omega \int_0^\infty G(t) \sin(\omega t)\, dt. \tag{23}$$

Substituting Eq. 21 into Eq. 23 we can obtain

$$S = \frac{2\Gamma(n)\sin(n\pi/2)G'(\omega)}{\pi\omega^n}, \tag{24}$$

where $\Gamma(n)$ is the Gamma function.

The power law is predicted by Martin et al.,[35] Rubinstein et al.,[36] Muthukumar,[39] and Winter et al.[40] It postulates that the longest relaxation time of the gel diverges with the same critical exponent from both side of the gel point. A general expression for n is given by

$$n = \frac{z}{k+z}. \tag{25}$$

When hydrodynamic interactions are completely screened out and the excluded volume effects are dominant in the cluster, we obtain

$$n = \frac{d}{d_f+2} \tag{26}$$

from Eqs. 17, 18, and 25. On the other hand, if excluded volume effects as well as hydrodynamic interactions can be completely screened out, n is expressed by

$$n = \frac{d(d+2-2d_f)}{2(d+2-d_f)} \tag{27}$$

from Eqs. 18 to 20 and 25.[39] If the power law of Eq. 22 holds in sufficiently wide range of ω at the gel point, the loss tangent, $\tan\delta$ at the gel point is given by

$$\tan\delta = \tan\left(\frac{n\pi}{2}\right) \tag{28}$$

from the Kramers–Kronig relation,[38] indicating that $\tan\delta$ is independent of ω at gel point and that its value depends only on n.

Figures 10 and 11 show changes in G' and G'' with time at fixed ω's after the quench to 183 °C. Figure 12 shows changes in $\tan\delta$ with time at fixed ω's after the quench to 183 °C. From the time change in $\tan\delta$, the gelation process can be divided into the following 3 stages with respect to a characteristic time,

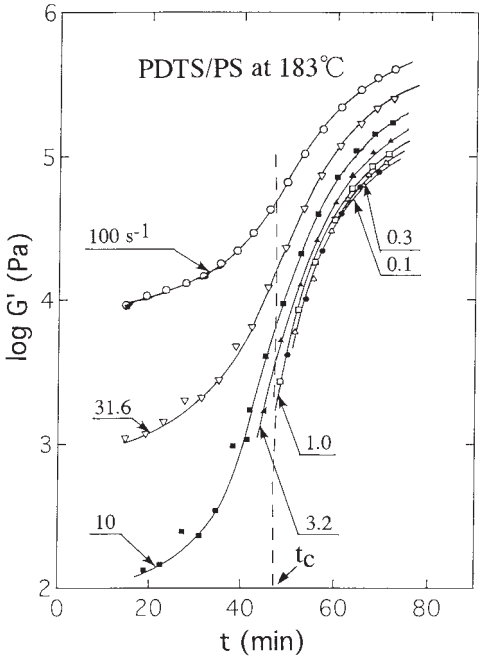

Fig. 10. Changes in G' at fixed ω's with t during the gelation process of the PDTS/PS system at 183 °C. t_c is gel point assessed from Fig. 12.

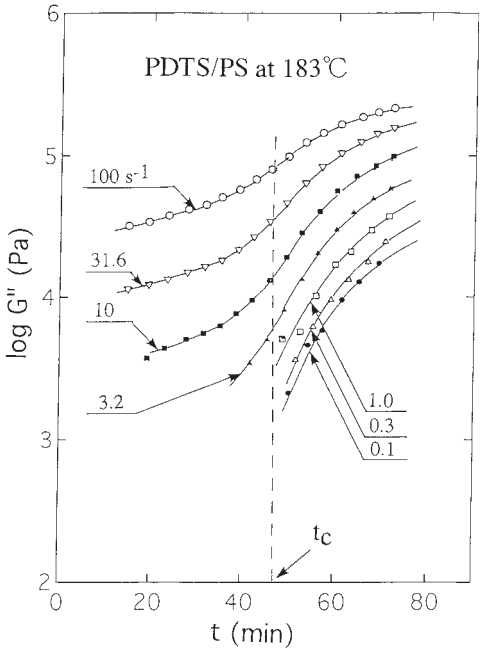

Fig. 11. Changes in G'' at fixed ω's with t during the gelation process of the PDTS/PS system at 183 °C. t_c is gel point assessed from Fig. 12.

t_c, for formation of the critical gel (t_c being 46.8 min at 183 °C, as will be given below):

(i) At $t < t_c$, G' increases more rapidly than G'', and thus $\tan\delta$ decreases rapidly with t. The $\tan\delta$ value is larger at lower ω's. In this region, PDTS forms the networks which are not macroscopically percolated yet. The clusters of the networks have the upper cut-off size ξ.

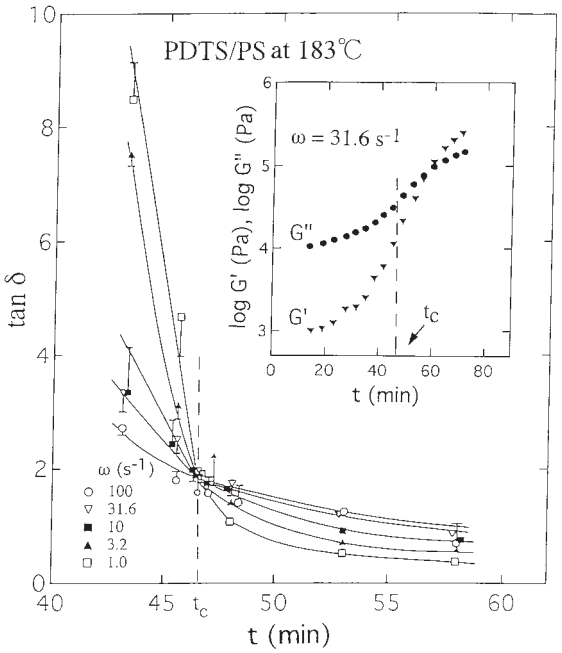

Fig. 12. Change in $\tan\delta$ at fixed ω's during the gelation process of the PDTS/PS system at 183 °C. Inset displays the changes in G' and G'' at $\omega = 31.6\ s^{-1}$ with t, where the vertical dashed lines indicate the gelation point ($t_c = 46.8$ min) at 183 °C.

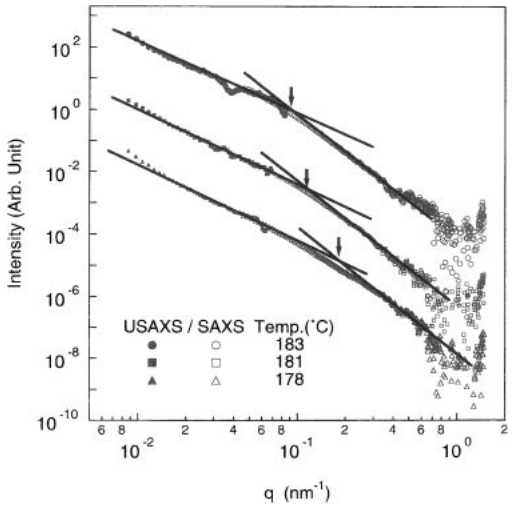

Fig. 13. Scattered intensity profiles of USAXS and SAXS for PDTS/PS system at 178, 181, and 183 °C. USAXS and SAXS profiles are shifted vertically so that they can be smoothly interconnected. Note that the USAXS and SAXS profiles are overlapping over a sufficiently large q-range. Allows indicate the crossover point q_c of the scattered intensity or the inverse of the lower limit of fractality in length scale.

Table 1. Characteristic Time for Formation of the Critical Gel or Gel Point t_c, Loss Tangent at t_c, $\tan\delta$, the Exponent n, n_{tan}, Obtained from $\tan\delta$ at Gel Point, or n_{slope}, Obtained from $\log_{10} G'$ and $\log_{10} G''$ vs $\log\omega$ Plot, and Gel Strength, S, at Each Temperature

Temp. /°C	T_c /min	$\tan\delta$	n_{tan}	n_{slope}	10^{-2} S /Pa s^n
183	46.8	1.84	0.68 ± 0.02	0.68 ± 0.02	9.93
181	29.0	1.84	0.68 ± 0.02	0.68 ± 0.02	19.8
178	16.7	1.63	0.65 ± 0.02	0.65 ± 0.02	23.0

(ii) At $t = t_c$, $\tan\delta$ becomes independent of ω. This indicates that the system has reached the gel point and that the cluster of the networks with macroscopically percolated or with infinitely large molecular weight is formed.

(iii) At $t > t_c$, the clusters are linked into three-dimensionally interconnected networks. G' still increases faster than G'' but its growth rate becomes moderate. As a result, $\tan\delta$ decreases gradually with t.

We estimated the values n, n_{slope} from the plots of $\log_{10} G'$ and $\log_{10} G''$ vs $\log_{10}\omega$ at gel point at each temperature and we list them in Table 1. The values of n_{slope} agree with those of n_{tan}, indicating that the experimental results confirm theoretical consistency. The estimated values of n are almost independent of temperature and agree with the value of 2/3 predicted by the percolation theory of Eq. 26 with $d_f = 2.5$.[35] Figure 13 shows scattering intensity profiles of USAXS and SAXS at gel point for 2.5 wt % PDTS/PS at 178, 181, and 183 °C. Fractal dimensions, $d_f = 2.5 \pm 0.1$, obtained from the structure factors and crossover wave numbers, q_c, are listed in Table 2. As the value of d_f obtained from structure factor

Table 2. Fractal Dimension d_f, $d_{f,sf}$, Obtained from the Scattered Intensity, and Crossover Wave Number q_c

Temp./°C	$d_{f,sf}$	q_c/nm^{-1}
183	2.40	0.11
181	2.49	0.13
178	2.58	0.22

coincides with that calculated by Eq. 26 for $n = 2/3$, the ramified structure made of PDTS fibrils in the gel for PS-60/2.5 has the following characteristic points: i) hydrodynamic interactions are completely screened out and ii) the excluded volume effects are significant.

While n is independent of the quench depth, S increases with decreasing temperature. This fact indicates that the fractal nature of the network structure of PDTS does not change with temperature, but that the mechanical strength of the fractal network increases with the decrease of the lower limit length scale of fractality with decreasing temperature.

We proved directly the self-similarity of evolving structures from in-situ and real time structure analysis during the gelation

process. Self-similarity in the cluster growth at a given ε is expected to give the mechanical self-similarity[41–43] as well. This self-similarity makes it possible to superpose angular frequency dependence of G' and G'' obtained at different p's ($p < p_c$) to give universal curves $G'a_v$ vs ωa_h and $G''a_v$ vs ωa_h, where a_v and a_h are, respectively, vertical and horizontal shift factors at each p. The shift factors a_v and a_h are defined by

$$a_v = \frac{J_e^0(p)}{J_e^0(p_r)} = \left[\frac{\varepsilon(p)}{\varepsilon(p_r)}\right]^{-z}, \tag{29}$$

and

$$a_h = \frac{\tau(p)}{\tau(p_r)} = \left[\frac{\varepsilon(p)}{\varepsilon(p_r)}\right]^{-(k+z)}, \tag{30}$$

where $\varepsilon(p_r)$ is the value ε at a given reference reaction extent p_r. From Eqs. 29 and 30, we can obtain

$$\frac{\log a_v}{\log a_h} = \frac{z}{k+z}, \tag{31}$$

indicating that $\log_{10} G'(\omega)$ and $\log_{10} G''(\omega)$ at different p's ($p < p_c$) can be superposed each other by shifting along a straight line with the slope of $z/(k+z)$. Figure 14 shows the results of the superposition of $\log_{10} G'(\omega)$ and $\log_{10} G''(\omega)$ vs ω at 183 °C obtained at various ε values before reaching the gel point. In order to obtain the master curves we shifted G' and G'' at each ε by the shift factors a_v and a_h with the constraints given by Eqs. 31 and 25. Namely, we shifted G' and G'' along the straight line with a slope $n = z/(k+z) = 0.68$. Here p is assumed to be proportional to t and hence ε is calculated from $\varepsilon = |t - t_c|/t_c$ with $t_c = 46.8$ min. We can obtain the master curves for G' and G'' measured at various ε values before reaching the gel point and we observe a $\omega^{2/3}$ power law at a high frequency region. When the system is close to the gelation point, very large clusters appear and smaller clusters may be considered as the matrix. This situation is very similar to the mechanical behavior of a dilute solution of polymers. The deviation of the mechanical behavior from the 2/3 power law of ω at the low frequency limit is due to the break of the self-similarity at the length scale greater than ξ and is attributed to the terminal flow behavior of the clusters as a whole.

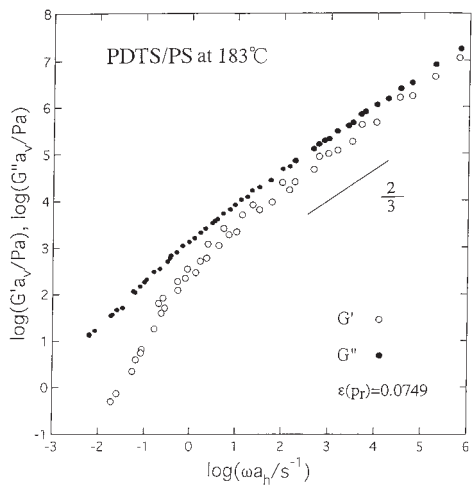

Fig. 14. Superposition of frequency dependence of G' and G'' obtained at various values of ε before gelation point along a straight line with a slope n at 183 °C.

The logarithmic shift factors $\log_{10} a_v$ and $\log_{10} a_h$ were plotted as functions of $\varepsilon(p)/\varepsilon(p_r)$. Each plot gives a straight line and the slope is $-z$ for $\log_{10} a_v$ and $-(k+z)$ for $\log_{10} a_h$. The values of k and z are 1.4 ± 0.1 and 3.1 ± 0.1, respectively. The crystallization of PDTS gives a larger value of z than the chemical gelation system such as end-linking polymers,[43] indicating that the PDST/PS system forms more dense networks than the chemical gels in which the gelation occurs by the chemical cross-linking reaction between the ends points of prepolymers. On the other hand, the gelation in our system occurs by crystallization of PDTS, so that the networks of PDTS systems consist of the fibrils of the crystalline structures of PDTS. The cross-linking reaction in chemical gels is restricted to the end points of prepolymers, while the physical "cross-linking" via crystallization of PDTS can occur at any points of fibrils. Thus, the PDTS system is expected to form more dense networks than the chemical gels.

2. Hierarchical Structures of PDTS Gel

The most stable stereo structure of a PDTS molecule and the network structure made of PDTS molecules formed accompanying sol–gel transition are already characterized as described in Sec. 1. In Sec. 2, we will investigate the PDTS fibril structure and then describe the hierarchical structure of PDTS gel. Figure 15 shows transmission electron micrographs (TEM) obtained for the freeze-dried 1.0 wt % concentration of PDTS/1,4-dioxane gel. From the TEM observation, the cross-sectional diameter of the proto-fibril is estimated to be 12 nm. Fibrils with a distribution of the cross-sectional diameter are composed of the proto-fibrils. Since the crystal structure of PDTS fibrils in gels was found to be independent of matrix materials from SAXS and WAXD profiles of their gels, we subsequently

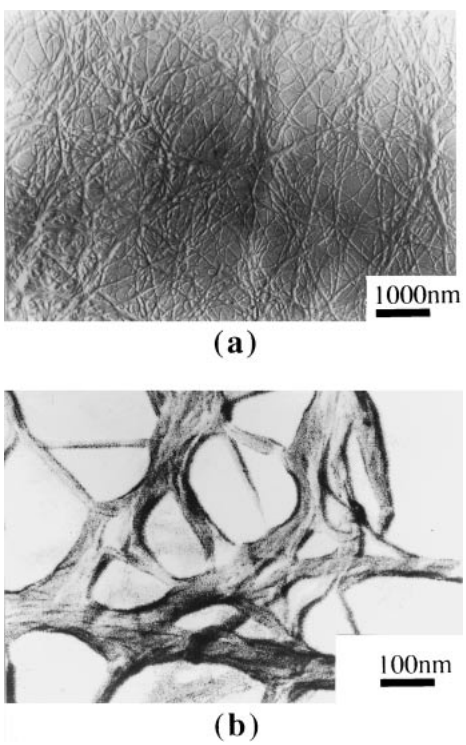

Fig. 15. TEM photographs (a, b) of freeze-dry-PDTS networks for the 1.0 wt % PDTS/1,4-dioxane gel.

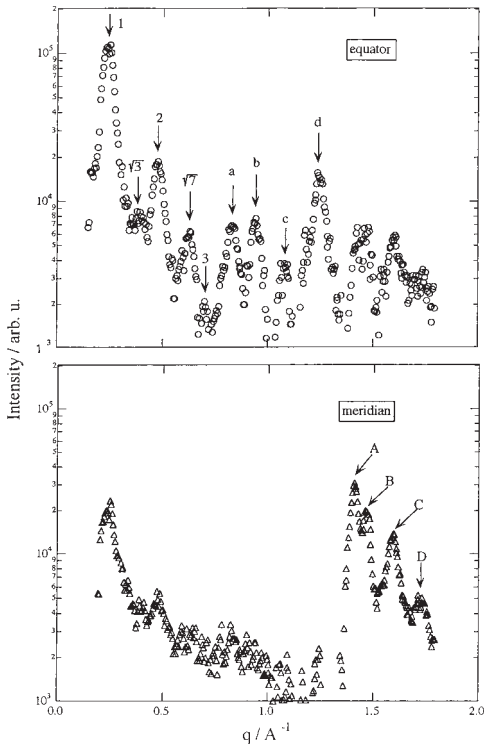

Fig. 16. SAXS and WAXD profiles of equator and meridian directions for the oriented 10 wt % PDTS/cross-linked SBR gel with draw ratio 1.7.

elucidated the crystal structure of the fibrils using a typical elongated PDTS gel. Figure 16 shows equator and meridian profiles of SAXS and WAXD for the elongated gel formed in 10 wt % concentration of PDTS/crosslinked SBR.[44] The oriented gel gives higher order scattering maxima, from which the crystal structure of PDTS fibrils was determined. The system of the crystal structure of PDTS in fibrils is hexagonal with symmetry of $6/m\ 2/m\ 2/m$ and the lattice cell constants $a = b = 30.2$ Å, $c = 4.4$ Å, and $\gamma = 120°$. As the crystal structure of the PDTS powder that was synthesized from D-sorbitol and *p*-methylbenzaldehyde is orthorhombic with $a = 20.4$ Å, $b = 17.6$ Å, and $c = 5.5$ Å, the crystal structure of PDTS fibrils in gels is different from that of PDTS powder. Thus PDTS has characteristics of polymorphism.

Two types of hierarchical structures of PDTS gel[45] (gel morphology) are formed, depending upon the gelation mechanism. Gel morphology (i) formed by S/L phase transition: This morphology is generally formed when quench depth $\Delta\Phi_{PDTS}$ or ΔT is shallow. PDTS crystalline clusters with a distribution of finite size are first formed by physical association of PDTS molecules, followed by the evolution into the infinite crystalline clusters, resulting in a gel where the amorphous liquids fill the space of the crystalline network structures. Gel morphology (ii) formed by competition with S/L phase transition and L/L phase transition: This morphology is generally formed when the quench depth $\Delta\Phi_{PDTS}$ or ΔT is deep. In this case, L/L phase separation into PDTS-rich domains and PDTS-poor domains evolves into bi-continuous network structures. The clusters evolve into the infinite cluster size in the PDTS-rich domain, maintaining the amorphous liquid in the space of the crystalline network structures in the gel. Morphology (ii) is dual,[45,46] one having a periodical concentration fluctuation based upon L/L phase separation with a characteristic length, Λ_m, the size of which depends on ΔT and $\Delta\Phi_{PDTS}$, and the other having the percolated crystalline network within the phase-separated domains. The crystalline network structures in gel morphology (i) and gel morphology (ii) are characterized with mass fractal dimensions having the upper cut-off length scale of around 12 μm and the lower cut-off length scale around 15 nm, where both scales depend on ΔT and $\Delta\Phi_{PDTS}$.

3. Self-Assembling Nucleators of PDTS for Highly Transparent i-PP

Figure 17 shows the dynamic storage modulus G' over all temperatures covered during cooling process from molten homogeneous state at 220 °C to crystallized state as well as during heating process from the crystallized state to the molten homogeneous state, both for 2.5 mol% polyethylene-*r*-isotactic-polypropylene (r-PP) neat polymer and 0.4 wt % PDTS/r-PP. The curves are quite different. The G' of molten neat r-PP at 220 °C increases smoothly with decreasing temperature and suddenly increases at $T_{c,neat} = 121$ °C, onset temperature of nucleation and growth of r-PP. The G' hardly changes at 100–135 °C and abruptly decreases at around 140 °C (line a) and then decreases smoothly at 160–210 °C (line b) with increase of temperature. Thus $T_{m,neat} = 151$ °C, the temperature of intersecting point between lines a and b, is the melting tem-

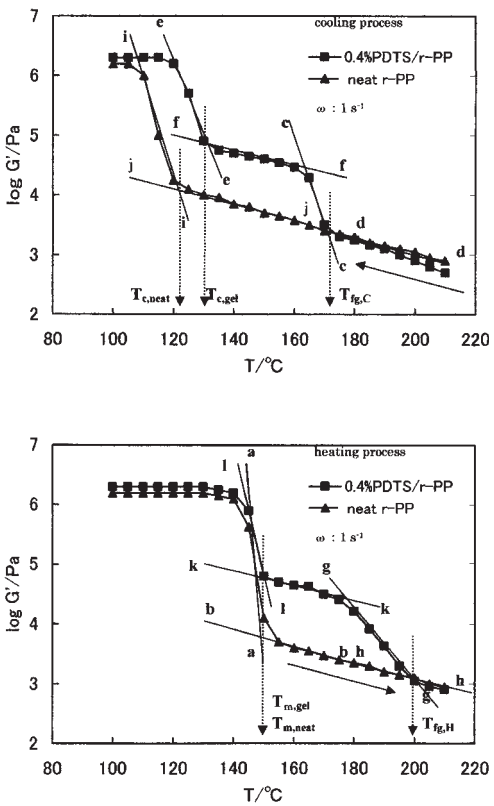

Fig. 17. Dynamic storage modulus G' over all temperatures covered during cooling process from molten homogeneous state to crystallized state as well as during heating process from the crystallized state to the molten homogeneous state for 2.5 mol% polyethylene-*r*-isotactic-polypropylene (r-PP) neat polymer and 0.4 wt % PDTS/r-PP.

perature of r-PP. On the contrary, G' of 0.4 wt % PDTS/r-PP jumps up two times, at 172 and 131 °C, during the cooling process. The network structure of PDTS will be formed at $T_{fg,c} = 172$ °C, the temperature of crossover point between lines c and d. T_c of r-PP will be increased from $T_{c,neat} = 121$ °C into $T_{c,gel} = 131$ °C, the temperature of the crossover point between lines e and f, by the nucleator effect of PDTS network structure. G' of 0.4 wt % PDTS/r-PP jumps down two times, at 151 and 201 °C, during the heating process. $T_{m,gel} = 151$ °C is the melting temperature of r-PP, which is equal to $T_{m,neat}$. $T_{fg,H} = 201$ °C, the temperature of crossover point between lines g and h, corresponds to the dissolution temperature of the PDTS network structure, as described in Sec. 3.1.

3.1 Dynamic Viscoelasticity of the PDTS and Molten i-PP Systems.[47,48] Dynamic viscoelastic responses were explored on i-PP melt ($M_v = 1.61 \times 10^5$, $M_w/M_n = 4.4$) and 0.3, 0.5, and 1.0 wt % PDTS/i-PP systems (P10, P13, P14, and P15, respectively) in order to clarify sol–gel transitions of PDTS in i-PP melt. Figures 18 and 19 show temperature dependencies of the storage modulus G' and the dynamic viscosity η' at $\omega = 0.1$, 1, 10, and 10^2 rad s^{-1}, during the cooling process, at the rate of 1 °C/min, from 250 to 140 °C for 1.0 wt % PDTS/i-PP (P15, curves a to d) and from 250 to 130 °C for bulk i-PP (P10, curves a′ to d′), respectively. At temperatures lower than about 201 °C, the lower the value of ω, the bigger the difference of G' between 1.0 wt % PDTS/i-PP and bulk i-PP, $\Delta G'$. The result for $\Delta G'$ indicates the formation of

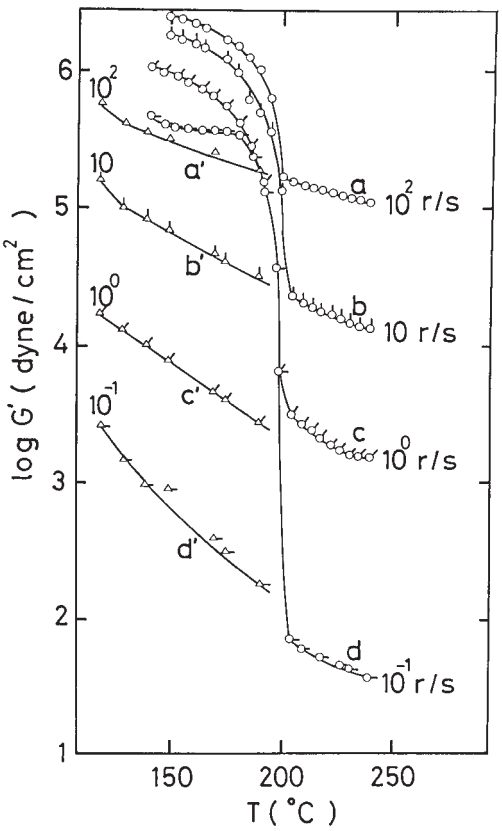

Fig. 18. Temperature dependencies of storage modulus G' which were measured during cooling process from 250 to 150 °C for 1.0 wt % PDTS/i-PP (P15, curves a to d) and from 250 to 130 for bulk i-PP (P10, curves a′ to d′).

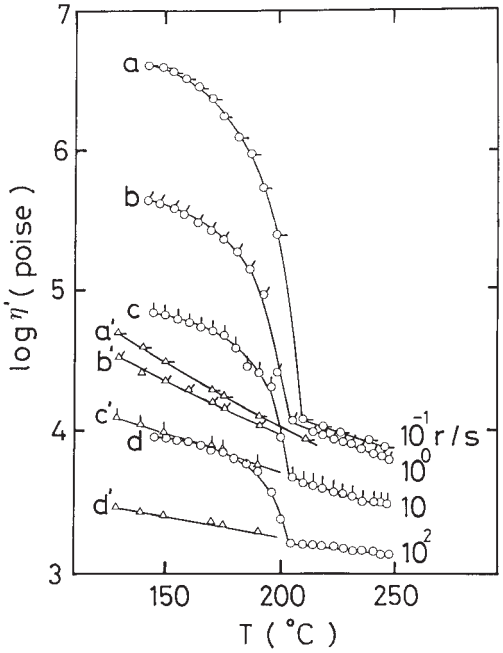

Fig. 19. Temperature dependencies of dynamic viscosity η' which were measured during cooling process from 250 to 150 °C for 1.0 wt % PDTS/i-PP (P15, curves a to d) and from 250 to 130 for bulk i-PP (P10, curves a′ to d′).

giant clusters of a large spatial scale. 1.0 wt % PDTS/i-PP has sol–gel transition temperature $T_{fg,c} = 201$ °C, which corresponds to the critical temperature for formation of PDTS percolation network via physical association of PDTS molecules. During the heating process from 150 to 214 °C, 1.0 wt % PDTS/i-PP has gel–sol transition temperature $T_{fg,H} = 212$ °C, which corresponds to the critical temperature for dissolution of PDTS percolation network formed by physical association of PDTS molecules and $T_{fg,H} > T_{fg,c}$.

The master curves of G' and η' are obtained for the sol and the gel temperature regions for P13, P14, and P15, assuming the themorheological simplicity in each region. Figure 20 shows master curves of G' and η' for P15 at reduced temperature $T_r = 175$ °C. Figure 21 indicates master curves of sol and gel of G' for P10, P13, P14, and P15 (left half) and the temperature dependencies of their shift factors (right half). The master curves for the sol regions of these systems are found to be identical with the ones of the bulk i-PP melt, implying that molecularly dispersed PDTS does not affect the dynamic response of molten matrix of i-PP. However, they were found to be quite different from those for the gel regions, especially at low reduced frequencies corresponding to the terminal flow region of the sol; the gel exhibits a plateau in the G' curve and a significant increase of η', namely, G''. These results imply that PDTS molecules form a macroscopic three dimensional network in the gel state. The loss tangent for the gel was found to be nearly equal to unity over all reduced frequencies covered in these experiments, implying that association and dissociation of PDTS molecules are in dynamic equilibrium, contributing to the large loss tangent. Figure 22 shows phase diagrams of PDTS/i-PP (a) and 1,3:2,4-dibenzylidenesorbitol (DBS)/i-PP (b) systems in parameter space T and PDTS concentration C.

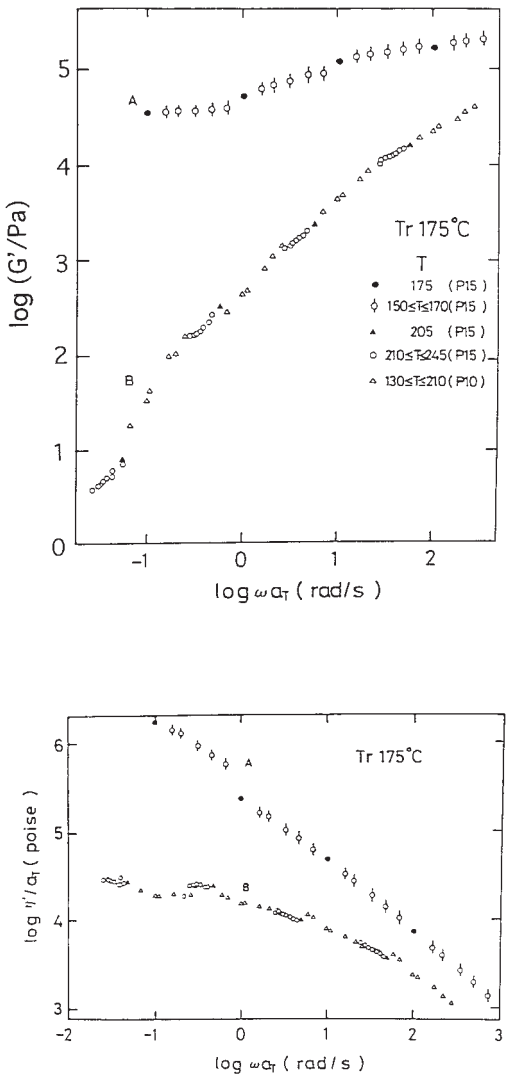

Fig. 20. Master curves of storage moduli G' and dynamic viscosities η' for both sol (curve B) and gel states (curve A) for 1.0 wt % PDTS/i-PP (P15) and for sol state for i-PP bulk (P10) (curve B). The reference temperature $T_r = 175$ °C. The symbols (●), (◌), (▲), and (○) represent G' and η' for 1.0 wt % PDTS/i-PP and (△) for i-PP bulk.

3.2 Random Crystallite Orientation of the α Form i-PP Sheet. In the molding processing of i-PP sheet, either monoclinic crystal (α form) or hexagonal crystal (β form) of i-PP can be predominantly induced by selection of nucleator.[49] Figure 23 shows WAXD patterns for Through, Edge, and End of the i-PP sheet, where the sheet of an upper half of the figure was prepared by injection molding of the 0.5 wt % PDTS/i-PP pellet at 180 °C. Since the gel state of the PP pellet was maintained without dissolution of the PDTS network at the molding temperature, we named this molding method "orientation-gel molding". The sheet of the lower half of the figure was prepared by injection molding of the same pellet at 250 °C. Scattering maxima of the WAXD patterns imply α form.[50] The Through, Edge, and End WAXD patterns in the upper half of the figure indicate that the crystallites are strongly oriented. It is estimated that both *c*-axis orientation and *a*-axis orientation[51] of the lamella of i-PP crystallites are induced on the PDTS fibrils, which are aligned along MD direction in i-PP melt. As the crystal form of the self-assembling PDTS fibrils is hexagonal, it is presumed that (100) of the hexagonal crystal of PDTS fibrils is the active surface for the nucleation of molten i-PP. On the contrary, the Through, Edge, and End WAXD patterns in the lower half of the figure are not only weak in intensity in comparison with those in the upper half of the figure but are also independent of azimuthal angle. Thus the lamellae of i-PP are randomly oriented in the i-PP sheet, whose diffraction is shown in the half of the figure. The random orientation of the crystallites is induced because the self-assembling structure of PDTS is randomly formed at $T_{fg,c}$ higher than crystallization temperature of i-PP, during the cooling process from homogeneous state at 250 °C, and the random orientated self-assembling structure of PDTS acts as nucleator for the nucleation of molten i-PP. These results imply that i) self-assembled PDTS structure induces selectively nucleation of α form in i-PP melt, that ii) the lamellae of i-PP formed for PDTS/i-PP systems have generally a random orientation, and that iii) orientation-gel injection molding for PDTS/i-PP systems induces *c*-axis crystallite orientation and *a*-axis crystallite orientation.

3.3 Morphology of the i-PP Induced by the Self-Assembled PDTS Structure. Kinetics of nucleation of i-PP induced by the self-assembled PDTS structure and optical microscope (OM) images and the two-dimensional light scattering Hv and Vv patterns of the i-PP sheet were measured in order to clarify the mechanism of heterogeneous nucleation of i-PP and the morphology of the i-PP induced by the self-assembled PDTS structure.

Kinetics of isothermal nucleation for 0–0.5 wt % PDTS/i-PP systems was investigated by differential scanning calorimetry (DSC).[5] Figures 24 and 25 show the Avrami plots, $\ln(-\ln\theta)$ vs $\ln t$, for virgin i-PP and 0.5 wt % PDTS/i-PP, respectively, where $1-\theta$ is relative crystallinity. Equation 32 designates the Avrami equation

$$\theta = \exp(-kt^n), \tag{32}$$

where k and n are a constant and the Avrami exponent, respectively. Stein and Misra[52,53] derived the following Eq. 33 based upon the famous sector model with respect to nucleation and growth of spherulites:

$$X(t) = 1 - \exp(At^5), \tag{33}$$

where $X(t)$ and A are the relative crystallinity at t and a constant, respectively. In this model, rodlike precursers evolve into sheaflike structures and then eventually into spherulites. The values of Avrami exponent 3.0 and 5.0 are obtained from the slope in Figs. 24 and 25, respectively. Thus homogeneous nucleation and three-dimensional growth of spherulite are satisfied for virgin i-PP, while heterogeneous nucleation and rod or sheaf in sector model growth are supported for 0.5 wt % PDTS/i-PP. Subsequently, the OM images and Hv and Vv patterns were obtained in order to compare them with the results from dynamics of nucleation. Figures 26 and 27 show the OM images and the Hv and Vv patterns quenched at 25 °C from 245 °C for virgin i-PP and 0.5 wt % PDTS/i-PP, respectively. The formation of spherulites is indicated by the OM image

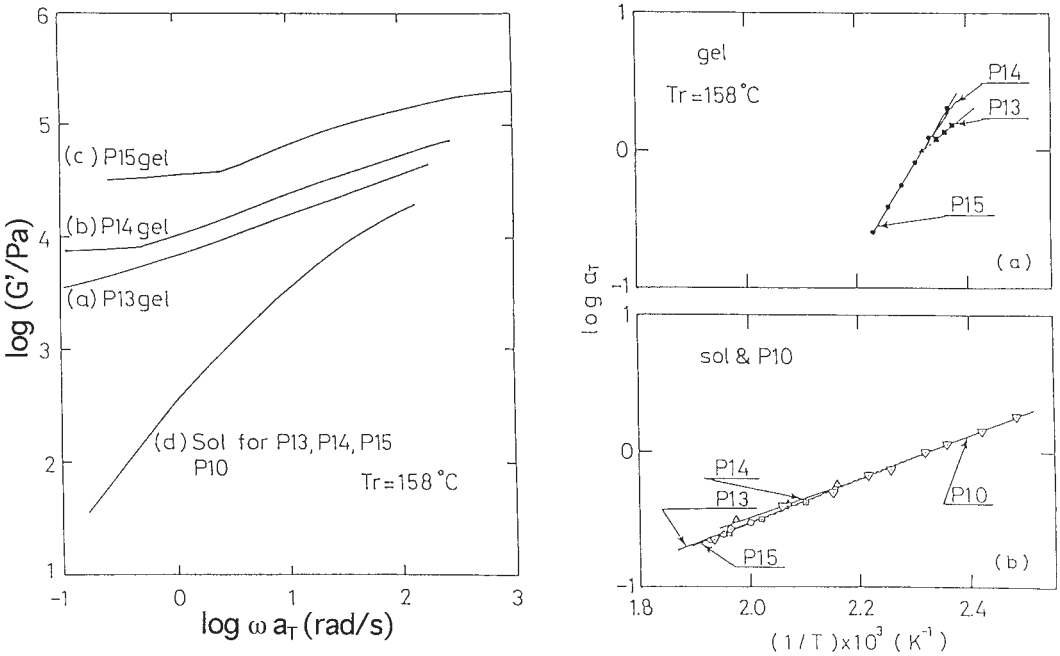

Fig. 21. The left half figure shows master curves for G' obtained for the gel states of (a) P13 (0.3 wt % PDTS/i-PP), (b) P14 (0.5 wt % PDTS/i-PP), and (c) P15 (1.0 wt % PDTS/i-PP), and for the sol states of (d) P13, P14, P15, and P10 (bulk i-PP) at $T_r = 158$ °C. The right half figures show temperature dependencies of the shift factors obtained for the gel state of P15 (filled circles), P14 (filled triangles), and P13 (filled squares) and for the sol states of P15 (open circles), P14 (open triangles), and P13 (open squares) and P10 (open inverted triangles) at $T_r = 158$ °C.

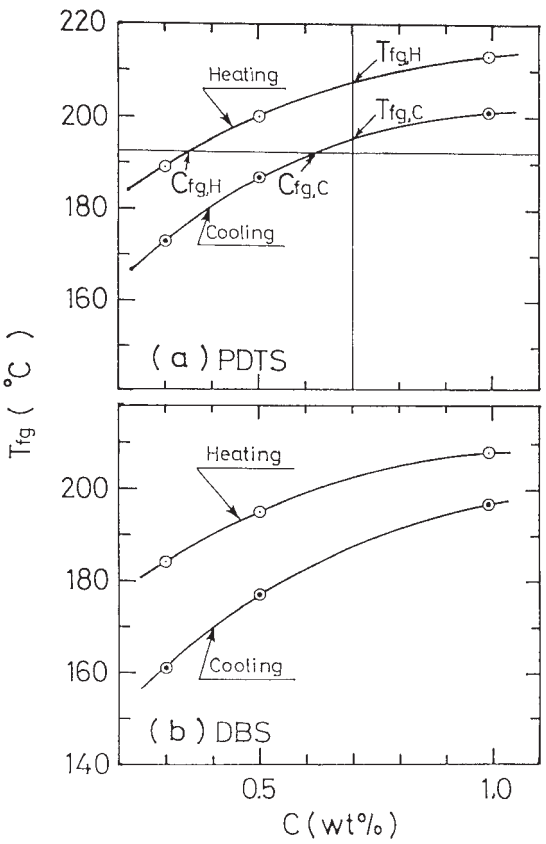

Fig. 22. Concentration dependence of the sol–gel transition temperatures T_{fg} for (a) PDTS/i-PP and (b) DBS/i-PP systems. The T_{fg}'s were obtained for both heating and cooling processes.

with the Maltese cross and the clover pattern of Hv for virgin i-PP in Fig. 26. The diameter of the spherulites is calculated to be 7.6 μm from the scattering maximum, θ_{max} on Hv, applying Eq. 33.[54]

$$4.09 = (4\pi/\lambda)R\sin(\theta_{max}/2), \quad (33)$$

where λ and R are the wave length of laser light and the radius of spherulites, respectively. On the other hand, the OM image and the Hv and Vv patterns for 0.5 wt % PDTS/i-PP are quite different from those of spherulites of virgin i-PP. The growth of spherulite from a nucleus of i-PP is stopped when its growing front impinges with the fronts of spherulites grown from neighbouring nuclei, resulting in the formation of grain boundaries. When the nucleation density is sufficiently large, the average size of the impinged spherulites becomes smaller than 1 μm. From the Hv pattern with monotonic decrease of the scattering intensity with θ, without scattering maximum, the lamellae build a sheaf-like superstructure with small apex angles.[55] Transparency of the sheet for 0.5 wt % PDTS/i-PP is higher than that of virgin i-PP, because scattering for 0.5 wt % PDTS/i-PP is remarkably weaker than that of virgin i-PP.

3.4 Effects of Concentration of PDTS Molecules on Properties of the i-PP Sheet. Figure 28 shows effects of the concentration of the self-assembling nucleators upon the transparency of the random i-PP (containing 2.5 mol% polyethylene) sheet with 1.0 mm thickness. The haze value of the i-PP sheet decreases dramatically from 56% for neat i-PP into 10% for the 0.2 wt % PDTS/i-PP, and decreases slowly with increase of PDTS concentration. Since the scattering from the self-assembled structure of PDTS molecules and from the crystallites is so weak, that transparency of the sheet is excellent. Optical properties of the sheet in terms of the transparency but also the

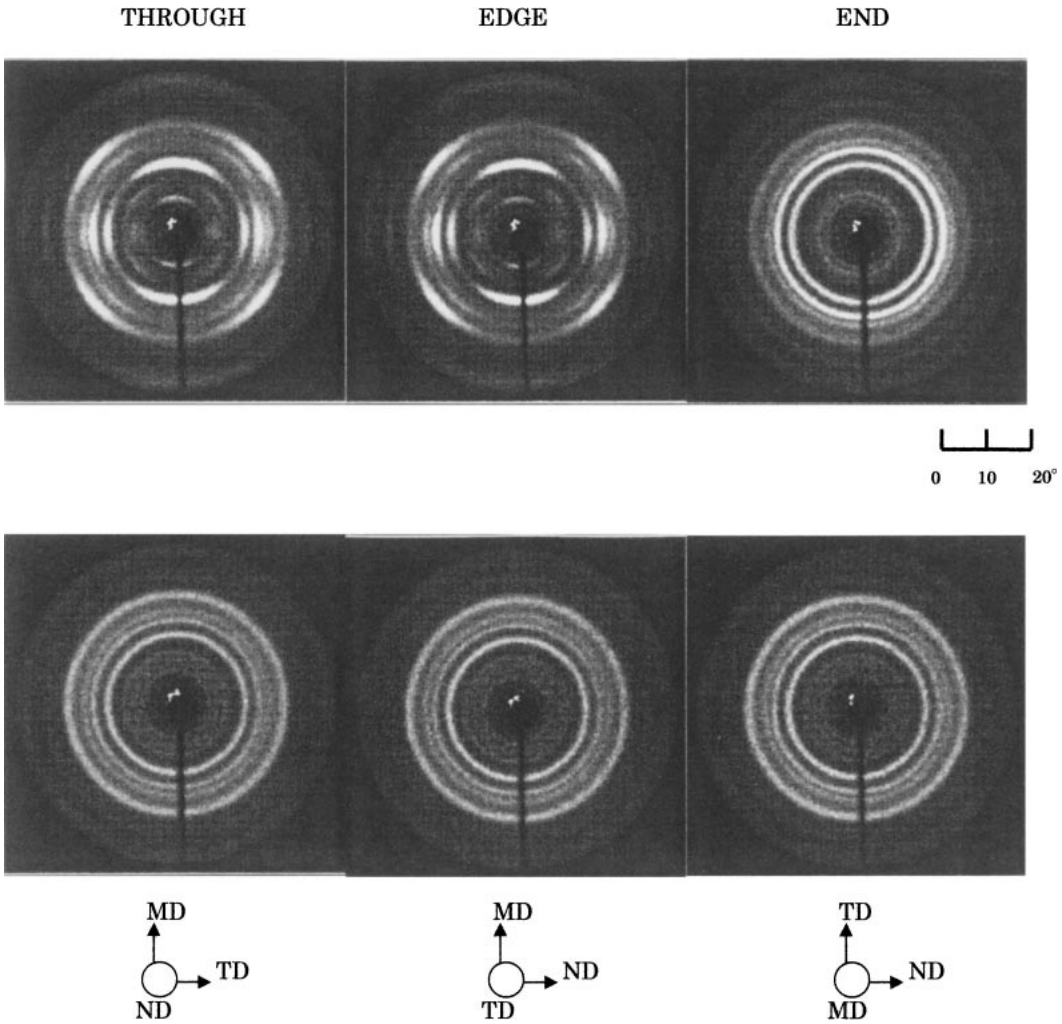

Fig. 23. Through, Edge, and End WAXD patterns for 0.5 wt % PDTS/i-PP sheet. The i-PP sheets of upper half of the figure and lower half of the figure were obtained by injection molding of the 0.5 wt % PDTS/i-PP pellet at 180 °C and 250 °C, respectively.

gloss of the surface of the sheet are remarkably improved by adding PDTS molecules. As the size of spherulites of i-PP decreases with increasing of the self-assembled PDTS molecules, the surface of the sheet becomes increasingly smooth; Consequently the gloss of the sheet should be improved. Since the remarkable improvement of optical properties of i-PP sheet was not possible so far, the new application fields of the transparent i-PP sheet will be wide, including fields such as disposable syringes, storage boxes, cases, and cups. The transparent grade of i-PP, which is by prepared mixing i-PP with the self-assembling nucleators in plant line of i-PP manufactures, has been developed not only in Japan but also in the world as the original excellent transparent i-PP. The volume of transparent grade of i-PP has been developed to about 10% of the total amount of i-PP in Japan and to about 6% of the total amount in the world. Mechanical properties of the sheet, such as flexural strength and modulus, and anisotropic shrinkage, are also improved.[56] Data of thermograms of differential scanning calorimeter (DSC) at the cooling rate of 20 °C/min show that the crystallization temperature T_c increases from 111 °C of neat i-PP to 128 °C for 0.3 wt % PDTS/i-PP, corresponding with the dynamic shear behavior in Fig. 17. T_c increases with increasing amount of PDTS or DBS up to 0.3 wt % concentration and saturates beyond 0.3 wt % concentration. The higher T_c, the shorter the mold processing time; therefore the cycle time of injection molding was shortened by 15–20%.

4. Conclusion

1,3:2,4-Bis-*O*-(*p*-methylbenzylidene)-D-sorbitol (PDTS) has been developed as a self-assembling nucleator, addition of which creates highly transparent semi-crystalline polypropylene. We clarified the self-assembling processes of PDTS and the formation of hierartical structures of PDTS in molten polymers and organic solvents. Two types of gel morphology are formed, depending upon the gelation mechanism. Gel morphology (i) formed by S/L phase transition; this morphology is generally formed when quench depth $\Delta\Phi_{PDTS}$ or ΔT is shallow. PDTS crystalline clusters with a distribution of finite size are first formed by physical association of PDTS molecules, followed by the evolution into the infinite crystalline clusters, resulting in a gel where the amorphous liquids fill the space of the crystalline network structures. Gel morphology (ii) formation involved a competition of two kinds of phase transition in the systems: S/L phase transition and L/L phase transition. This morphology is generally formed when quench depth $\Delta\Phi_{PDTS}$ or ΔT is deep. In this case, L/L phase separation into

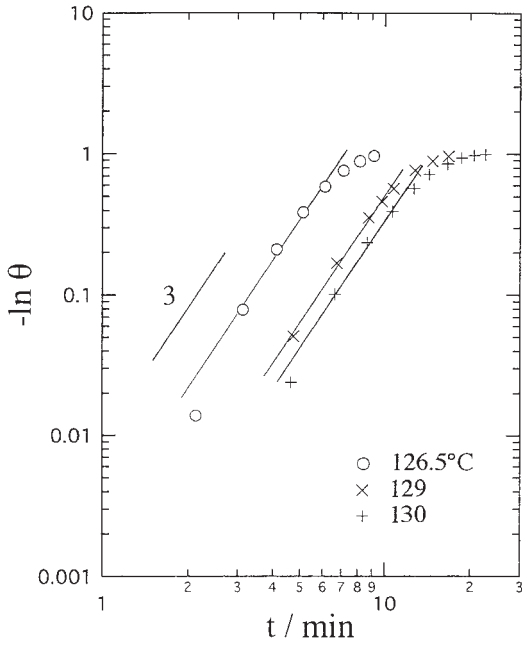

Fig. 24. Avrami plots, $\ln(-\ln\theta)$ vs $\ln t$, of the isothermal crystallization at 126.5, 129, and 130 °C for virgin i-PP, where $1-\theta$ is relative crystallinity of i-PP.

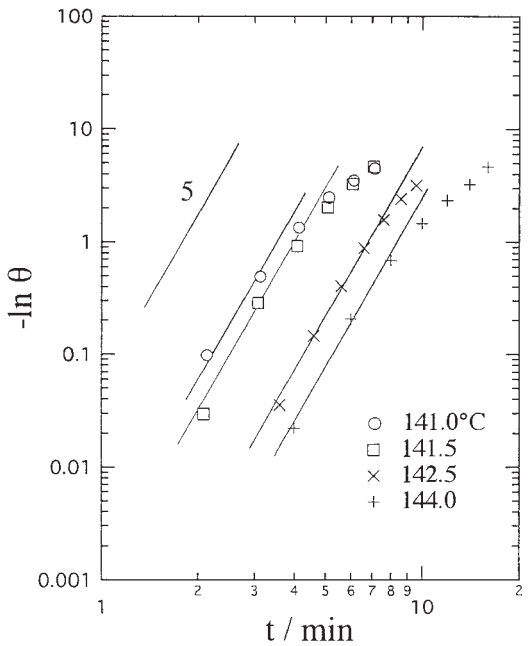

Fig. 25. Avrami plots, $\ln(-\ln\theta)$ vs $\ln t$, of the isothermal crystallization at 141.0, 141.5, 142.5, and 144.0 °C for 0.5 wt % PDTS/i-PP, where $1-\theta$ is relative crystallinity of i-PP.

PDTS-rich domains and PDTS-poor domains first evolves into bi-continuous network structures via the early stage of spinodal decomposition, followed by formation of gel networks of PDTS in the PDTS-rich domains. Morphology (ii) is therefore dual, one having a periodical concentration fluctuation originating from L/L phase separation with a characteristic length, Λ_m, the size of which depends on ΔT and $\Delta\Phi_{PDTS}$, and the

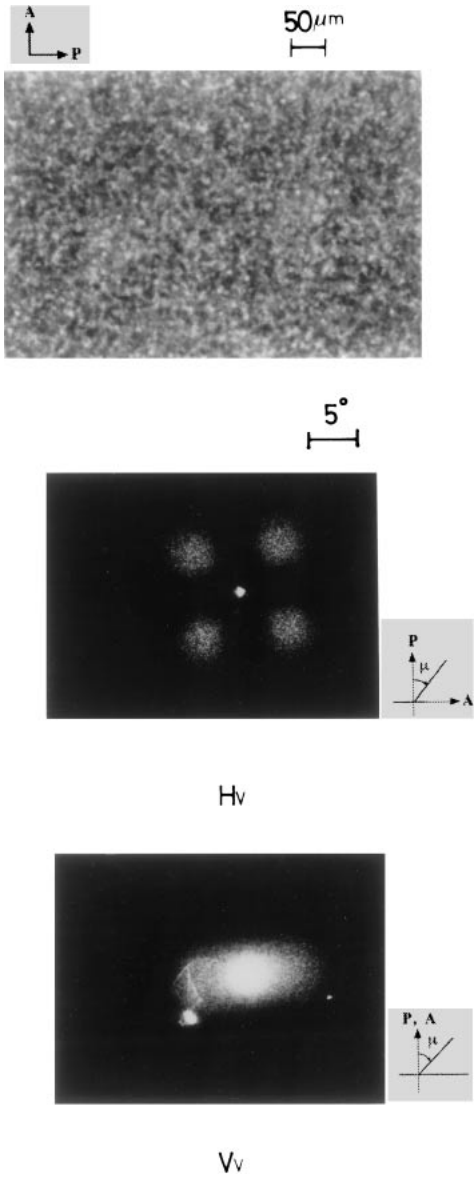

Fig. 26. OM images and the two-dimensional light scattering Hv and Vv patterns quenched at 25 °C from 245 °C for virgin i-PP.

other having the percolated crystalline network within the phase-separated domains. The crystalline network structures in gel morphology (i) and gel morphology (ii) are characterized with mass fractal dimensions having the upper cut-off length scale of around 12 μm and the lower cut-off length scale around 15 nm, where both scales depend on ΔT and $\Delta\Phi_{PDTS}$. The system of the crystal structure of PDTS fibrils is hexagonal with symmetry of $6/m\ 2/m\ 2/m$ and the lattice cell with $a = b = 30.2$ Å, $c = 4.4$ Å, and $\gamma = 120°$. In the case of 0.2–0.5 wt % PDTS/i-PP, the self-assembling structure of PDTS is formed at $T_{fg,c}$ higher than T_c in molten polypropylene during the cooling process. The self-assembling structure of PDTS has the following characteristics: i) large specific surface area, ii) random orientation, and iii) active nucleator for the nucleation of molten i-PP. Thus the i-PP has the following properties: i) excellent transparency, so that the lamellae can

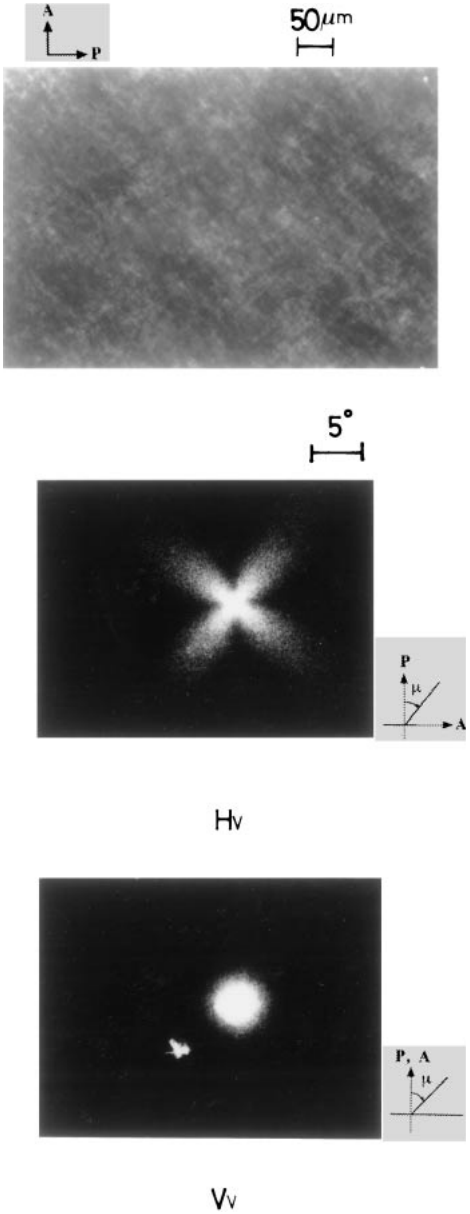

Fig. 27. OM images and the two-dimensional light scattering Hv and Vv patterns quenched at 25 °C from 245 °C for 0.5 wt % PDTS/i-PP.

build a sheaf-like crystalline superstructure with a small apex angle; ii) iso-directional and improved mechanical properties; and iii) shortened molding time.

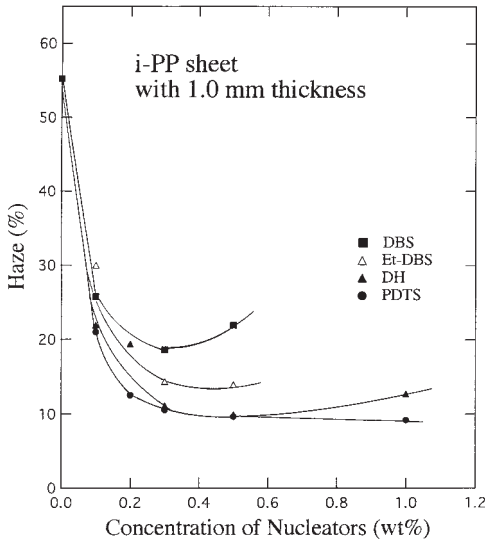

Fig. 28. Effects of concentration of the self-assembling nucleators on transparency of the random i-PP (containing 2.5 mol% polyethylene) sheet with 1.0 mm thickness. Chemical structures of Et-DBS and DH are respectively 4,4′-ethyl substituted-DBS and mixtures of 1,3-*O*-(*o*,*p*-dimethylbenzylidene):2,4-*O*-benzylidene-D-sorbitol and 1,3-*O*-benzylidene:2,4-*O*-(*o*,*p*-dimethylbenzylidene)-D-sorbitol.

References

1 F. L. Binsbergen, *J. Polym. Sci., Polym. Symp.*, **59**, 11 (1977); H. N. Beck, *J. Appl. Sci.*, **9**, 2131 (1965).

2 M. Fujiyama, H. Awaya, and S. Kimura, *J. Appl. Polym. Sci.*, **22**, 1001 (1977).

3 S. N. Garg and R. S. Stein, "Crystallization and Morphology of Nucleated Polymers," Proc. ANTEC, N. Y. (1988), p. 1021.

4 T. Kobayashi, H. Hasegawa, and T. Hashimoto, *J. Soc. Rheol., Jpn.*, **17**, 86 (1989).

5 "Advanced Technology of Additives for Polymers," CMC, Jpn. (1988), p. 204.

6 P. J. Flory, *Faraday Discuss. Chem. Soc.*, **57**, 1 (1974).

7 P. G. de Gennes, *J. Phys., Lett.*, **37L**, 61 (1976).

8 D. Stauffer, *J. Chem. Soc., Faraday Trans. 2*, **72**, 1354 (1976); D. Stauffer, A. Coniglio, and M. Adam, *Adv. Polym. Sci.*, **44**, 103 (1982).

9 R. M. Hikmet, S. Calliter, and A. Keller, *Polymer*, **29**, 1378 (1988).

10 N. Kitabatake, H. Hatta, and E. Doi, *Agric. Biol. Chem.*, **51**, 771 (1987).

11 P. G. de Gennes, "Scaling Concepts in Polymer Physics," Cornell Univ. Press, Ithaca, New York (1979); D. Stauffer, "Introduction to Percolation Theory," Taylor & Francis, London & Philadelphia (1985).

12 T. Tachibana, T. Mori, and K. Hori, *Bull. Chem. Soc. Jpn.*, **53**, 1714 (1980).

13 J. W. Wolfe, R. M. Hann, and C. S. Hudson, *J. Am. Chem. Soc.*, **64**, 1493 (1942).

14 P. J. Terech, *Colloid Inter. Sci.*, **107**, 244 (1985); C. D. Adam, J. A. Durrant, M. R. Lowry, and G. J. T. Tiddy, *J. Chem. Soc., Faraday Trans. 1*, **80**, 789 (1984); Y.-C. Lin, B. Kachar, and R. G. Weiss, *J. Am. Chem. Soc.*, **111**, 5542 (1989).

15 M. Hoshino, *Junkatsu*, **19**, 292 (1974).

16 T. Kobayashi and K. Ando, USP 6187842 (2001).

17 K. Yoza, N. Amanokura, Y. Ono, T. Akao, H. Shinmori, M. Takeuchi, S. Shinkai, and D. N. Reinhoudt, *Chem.—Eur. J.*, **5**, 2722 (1999).

18 C. M. Grarner, P. Terech, J.-J. Alleegraud, B. Mistrot, P. Nguyen, A. de Geyer, and D. Rivera, *J. Chem. Soc., Faraday Trans.*, **94**, 2173 (1998); P. Terech, J. J. Allegraud, and C. M. Garner, *Langmuir*, **14**, 3991 (1998).

19 K. Sakamoto, R. Toshida, M. Hatano, and T. Tachibana, *J. Am. Chem. Soc.*, **100**, 6898 (1978).

20 J.-H. Fuhrhop, P. Schnieder, E. Boekema, and W. Helfrich, *J. Am. Chem. Soc.*, **110**, 2861 (1988).

21 K. Hanabusa, R. Tanaka, M. Suzuki, M. Kimura, and H. Shirai, *Adv. Mater.*, **9**, 1095 (1997).
22 M. Aoki, K. Nakashima, H. Kawabata, S. Tsutsui, and S. Shinkai, *J. Chem. Soc., Perkin Trans. 2*, **1993**, 347.
23 L. Lu and R. G. Weiss, *Chem. Commun.*, **1996**, 2029.
24 D. J. Abdallah, L. Lu, and R. G. Weiss, *Chem. Mater.*, **11**, 2907 (1999).
25 N. Amanokura, Y. Kanekiyo, S. Shinkai, and D. Reinhoudt, *J. Chem. Soc., Perkin Trans. 2*, **1999**, 1995.
26 M. Watase, Y. Nakatani, and H. Itagaki, *J. Phys. Chem. B*, **103**, 2366 (1999).
27 J. van Esch, S. D. Feyter, R. M. Kellogg, F. D. Schryver, and B. L. Feringa, *Chem.—Eur. J.*, **3**, 1238 (1997); J. van Esch, F. Schoonbeek, M. de Loos, H. Kooijman, A. l. Spek, R. M. Kellogg, and B. L. Feringa, *Chem.—Eur. J.*, **5**, 937 (1999).
28 Y.-C. Lin, B. Kachar, and R. G. Weiss, *J. Am. Chem. Soc.*, **111**, 5542 (1989).
29 N. L. Allinger, *J. Am. Chem. Soc.*, **99**, 8127 (1977).
30 T. Kobayashi, H. Yagi, S. Kitagawa, Y. Kawashima, and T. Hashimoto, *J. Chem. Soc. Jpn.*, **1993**, 850.
31 T. Kobayashi, S. Kitagawa, H. Yagi, K. Fujitani, S. Sakai, and T. Hashimoto, *J. Chem. Soc. Jpn.*, **1994**, 713.
32 T. Kobayashi, M. Takenaka, K. Saijo, and T. Hashimoto, *J. Colloid Interface Sci.*, **262**, 456 (2003).
33 J. W. Cahn, *J. Chem. Phys.*, **42**, 93 (1965).
34 M. Takenaka, T. Kobayashi, T. Hashimoto, and M. Takahashi, *Phys. Rev. E*, **65**, 041401 (2002).
35 J. E. Martin, D. Adolf, and J. P. Wilcoxon, *Phys. Rev. A*, **39**, 1325 (1989).
36 M. Rubinstein, R. H. Colby, and J. R. Gillmor, *Polym. Prepr.*, **30**, 81 (1989); "Space-Time Organization in Macromolecular Fluids," ed by F. Tanaka, M. Doi, and T. Ohta, Springer-Verlag, Berlin (1989).
37 H. H. Winter and M. Mours, *Adv. Polym. Sci.*, **134**, 165 (1997).
38 J. D. Ferry, "Viscoelastic Properties of Polymers," 3rd ed, Wiley, New York (1980).
39 M. Muthukumar, *J. Chem. Phys.*, **83**, 3162 (1985); M. Muthukumar, *Macromolecules*, **22**, 4656 (1989).
40 W. Hess, T. A. Vilgis, and H. H. Winter, *Macromolecules*, **21**, 2536 (1988).
41 F. Hodgson and E. I. Amis, *Macromolecules*, **23**, 2512 (1990).
42 R. Mullen, E. Gerard, P. Dugand, P. Rempp, and Y. Gnanou, *Macromolecules*, **24**, 1321 (1991).
43 M. Takahashi, K. Yokoyama, and T. Masuda, *J. Chem. Phys.*, **101**, 798 (1994).
44 T. Kobayashi, M. Takenaka, and T. Hashimoto, *Jpn. J. Polym. Sci. Technol.*, **55**, 613 (1998).
45 A. Onuki, "Phase Transition Dynamics," Cambridge (2002).
46 M. Doi and A. Onuki, "Polymer Physics・Phase Transition Dynamics," Modern Physics 19, Iwanami (1992).
47 T. Kobayashi, M. Takahashi, and T. Hashimoto, *J. Soc. Rheol., Jpn.*, **17**, 155 (1989).
48 T. Kobayashi, M. Takahashi, and T. Hashimoto, *J. Soc. Rheol., Jpn.*, **18**, 44 (1990).
49 T. Kobayashi and N. Ikeda, *Converting Technol.*, **24**, 47 (1996).
50 G. Natta and P. Corradini, *Nuovo Cimento, Suppl.*, **15**, 40 (1960).
51 S. Okatsu, "Base of Functional Materials for Polymer and Application," Technology Education Publication (2000), p. 146.
52 R. S. Stein and A. Misra, *J. Polym. Sci., Polym. Phys. Ed.*, **11**, 109 (1973).
53 R. S. Stein and M. B. Rhodes, *J. Appl. Phys.*, **31**, 1873 (1960).
54 M. B. Rhodes and R. S. Stein, *J. Polym. Sci., Part A*, **7**, 1539 (1969).
55 A. Misra and R. S. Stein, *J. Polym. Sci., Part B*, **10**, 473 (1972).
56 T. A. Shepard, C. R. Delsorbo, R. M. Louth, J. L. Walborn, D. A. Norman, N. G. Harvey, and R. J. Spontak, *J. Polym. Sci., Part B: Polym. Phys.*, **35**, 2617 (1997).

Toshiaki Kobayashi was born in Nagano, Shinshu, Japan, in 1943. He graduated from the Department of Synthetic Chemistry, Faculty of Engineering, Nagoya University in 1966, and received his M.Eng. from Nagoya University in 1969. He was awarded Ph.D. from Kyoto University in 2005. He joined Research & Development of New Japan Chemical Corp. (NJC) in 1966. He developed the industrial gelator of dibenzylidene sorbitol (DBS) in 1972. Invention Prize for Encouragement was given for the Patent of the nucleators of *o*-, *m*-, or *p*-methyl substituted DBS's and their polyolefin composition in 1985 sponsored by Jap. Institute of Invention & Innovation. Industrial Technology Award was given for the development of the self-assembling nucleators of a series of sorbitol derivatives for transparent *isotactic*-polypropylene in 2003 sponsored by Osaka Industrial Research Association. He retired from NJC in 2004. His current interests are synthesis of functional small-molecule-chemicals, research of higher order structures made of them, and their applications to polymer industry.